ABSTRACT

MICROSTRIP ZERO-SUM ANTENNA; CAD AND EXPERIMENTAL STUDY

by
Tuan H. Lam

A microstrip antenna array consisting of two elements combined with a stripline hybrid (rat-race) ring coupler is used to implement a zero-sum antenna. Numerical optimization of individual antenna elements in terms of feed location and patch size was achieved using IE3D (Zeland Software Inc., Fremont, CA), a fullwave 3-D planar electromagnetic simulation software. Further, design of a hybrid (rat-race) ring coupler in a stripline environment was carried out, yielding the sum and difference functions as 0.5 dB and 40 dB, respectively. A combination of a two-element antenna array and a hybrid (rat-race) ring coupler as a zero sum antenna has been studied numerically revealing that 40 dB differences can be expected between the sum and difference patterns in the forward direction at the operating frequency. Experimental results using MC5 material (ε_r=3.26 and thickness t=60 mils) (Glasteel Industrial Laminates, Collierville, TN) have shown that satisfactory performance can be achieved at the chosen operating frequency f=2.254 GHz.

MICROSTRIP ZERO-SUM ANTENNA; CAD AND EXPERIMENTAL STUDY

by
Tuan H. Lam

A Thesis
Submitted to the Faculty of
New Jersey Institute of Technology
in Partial Fulfillment of the Requirements for the Degree of
Master of Science in Electrical Engineering

Department of Electrical and Computer Engineering

October 1997

APPROVAL PAGE

MICROSTRIP ZERO-SUM ANTENNA;
CAD AND EXPERIMENTAL STUDY

Tuan Hong Lam

Dr. Edip Niver, Thesis Advisor — Date
Associate Professor of Electrical and Computer Engineering, NJIT

Dr. Sol Rosenstark, Committee Member — Date
Professor of Electrical and Computer Engineering, NJIT

Dr. Constantine Manikopulous, Committee Member — Date
Associate Professor of Electrical and Computer Engineering, NJIT

BIOGRAPHICAL SKETCH

Author: Tuan Hong Lam

Degree: Master of Science

Date: October 1997

Undergraduate and Graduate Education:

Master of Science in Electrical Engineering,
New Jersey Institute of Technology, Newark, NJ, 1997

Bachelor of Science in Electrical Engineering,
Rutgers University, Pitscataway, NJ, 1986

Major: Electrical Engineering

ACKNOWLEDGEMENT

I am deeply graceful to my thesis and academic adviser, Dr. Edip Niver, for his kindness, research guidance, stimulating suggestions, physical insight, expertise in electromagnetics, and especially his precious time.

Appreciation also goes to Dr. Jian-X. Zheng of Zeland Software Inc. for providing the electromagnetic simulation software and to Chuck Ludwig and Philip Johnson of Glasteel Industrial Laminates for the PC materials to fabricate the zero-sum antenna. Also suggestions on zero-sum antenna from Arthur Walier of TEC Electronics Corporation are acknowledged. Additional thanks to Rajesh Kapadia for his efforts in fabricating the coupler and the antenna elements.

TABLE OF CONTENTS

TABLE OF CONTENTS
(Continued)

LIST OF FIGURES

Figure **Page**

LIST OF FIGURES
(Continued)

Figure **page**

LIST OF FIGURES
(Continued)

Figure **page**

CHAPTER 1

INTRODUCTION

Advances in printed circuits materials have created a significant amount of interest in research and development of microstrip antennas. Microstrip antennas have found use in many applications due to their light weight, compact size, rugged, conformal characteristics and often lower costs in materials and mass production. Here, microstrip and stripline technologies will be used in a combination of an antenna and coupling configuration in the implementation of a zero-sum antenna operating at various frequencies, i.e. f=2.254 GHz. The zero-sum antenna considered in this work has been used at 1030 MHz and 1090 MHz for monopulse radar applications in avionics.

1.1 Zero-sum Antenna

Due to size restriction in the field application of the zero-sum antennas, the microstrip technology offers a suitable solution. The zero-sum antenna considered in this work consists of the following; a dual probe-fed microstrip patch antennas and a stripline hybrid ring coupler. The schematic structure of the zero-sum antenna is shown in Figure 1.1.

Two microstrip patches are placed at a distance of a half wavelength apart and function as radiating elements. Because an antenna is a bi-directional device, zero-sum antenna could operate both as a receiving and a transmitting antenna. The two radiating patches will also be used to receive the signals from an active source or a scattered signal from a passive target.

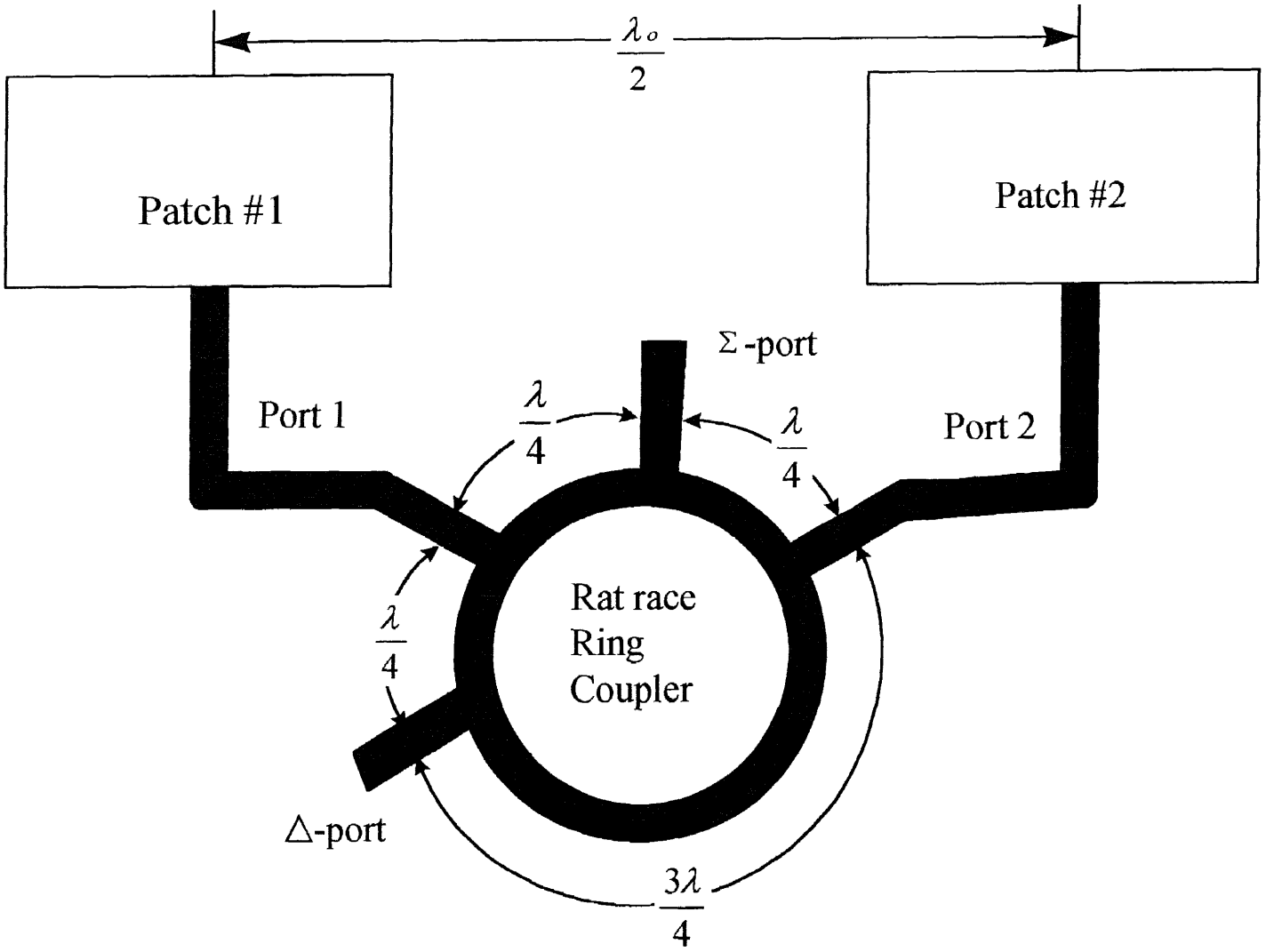

Figure 1.1 Functional schematic diagram of a zero-sum microstrip antenna

The rat-race ring coupler [1] is a four port device and its diagram is shown in Figure 1.1. Among the four ports, two of them will be used to feed the antenna elements. The third port will function as a sum port which effectively adds up the two signals received by the antenna elements and the last port is the difference port which effectively subtracts the two input signals received by the antenna elements, respectively.

The zero-sum antenna operation can be explained in terms of a simple antenna array consisting of two elements. Although the general explanation is based on point source elements which radiate in all directions, the microstrip elements considered in this thesis radiate into a half space only.

1.2 Two Isotropic Point Sources of Equal Amplitude and Phase

Consider two isotropic point sources [2] having excited by equal amplitudes and phases be separated by a distance d as shown in Figure 1.2 (a). The total field at observation point P can be expressed as:

$$E_{tot} = E_0 \frac{e^{-jkr_1}}{r_1} + E_0 \frac{e^{-jkr_2}}{r_2}$$

where $r_1 \cong r - \frac{d}{2}\cos\phi$ and $r_2 \cong r + \frac{d}{2}\cos\phi$

then the total field can expressed as:

$$E_{tot} \cong E_0 \frac{e^{-jkr}}{r}\left(e^{j\frac{kd\cos\phi}{2}} + e^{-j\frac{kd\cos\phi}{2}}\right)$$

$$\cong 2E_0 \frac{e^{-jkr}}{r}\cos\left(\frac{kd\cos\phi}{2}\right)$$

If $d = \frac{\lambda}{2}$ then $kd = \frac{2\pi}{\lambda}\cdot\frac{\lambda}{2} = \pi$

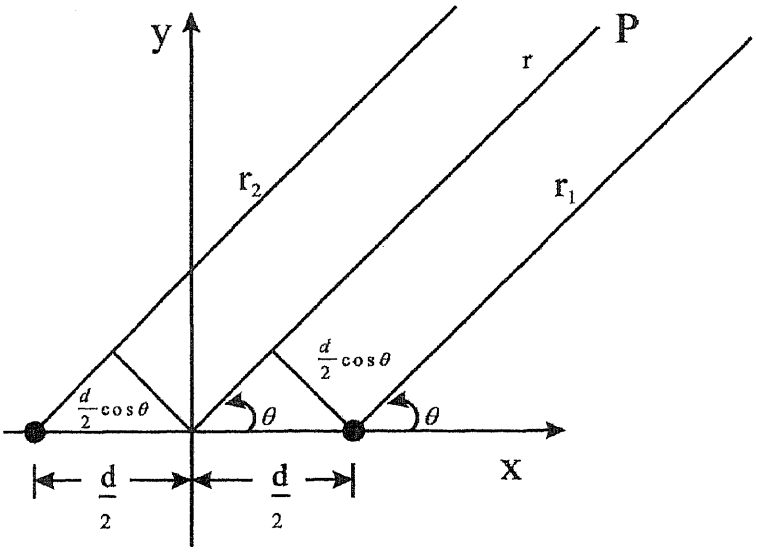

a) Two isotropic point sources currents spaced one-half wave length apart.

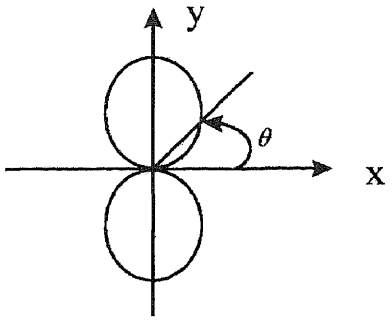

b) Polar plot of array factor $AF(\theta) = \cos\left[(\pi/2)\cos\theta\right]$ of equal amplitudes and phases.

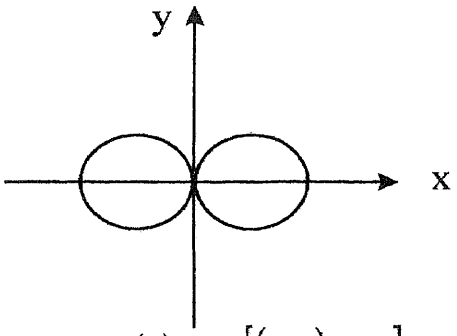

c) Polar plot of array factor $AF(\theta) = \sin\left[(\pi/2)\cos\theta\right]$ of equal amplitudes and opposite phases.

Figure 1.2 Two element antenna array

The array factor (AF) is equal to:

$$AF(\phi) = \cos\left(\frac{kd}{2}\cdot\cos\phi\right) = \cos\left(\frac{\pi}{2}\cdot\cos\phi\right)$$

and is plotted in Figure 2(b). This array factor with a main lobe in the forward direction corresponds to the sum part of the zero-sum antenna operation.

1.3 Two Isotropic Point Sources of Equal Amplitude but Opposite Phase

Now, consider two isotropic point sources having excited by equal amplitudes but opposite phases are placed at a distance d as shown in Figure 1.2 (a). Then the total field can be expressed as:

$$E_{tot} = E_0\cdot\frac{e^{-jkr_1}}{r_1} - E_0\cdot\frac{e^{-jkr_2}}{r_2}$$

$$\cong E_0\cdot\frac{e^{-jkr}}{r}\cdot 2j\cdot\frac{e^{-jk\cdot\frac{d}{2}\cdot\cos\phi} - e^{j\cdot\frac{kd}{2}\cdot\cos\phi}}{2j}$$

$$\cong -2j\cdot E_0\cdot\frac{e^{-jkr}}{r}\cdot\sin\left(\frac{kd}{2}\cdot\cos\phi\right)$$

Therefore array factor AF for this case becomes:

$$AF(\phi) = \sin\left(\frac{kd}{2}\cdot\cos\phi\right) = \sin\left(\frac{\pi}{2}\cdot\cos\phi\right)$$

This corresponds to the difference action of the zero-sum antenna operating with a null in the forward direction and is plotted in Figure 2(c).

1.4 The Hybrid (Rat-Race) Coupler

The hybrid (rat-race) coupler shown in Figure 1.1 is used to excite the radiating elements discussed previously either in phase or out of phase, depending on how the source is connected. If ports 1 and 2 are excited with in phase signals, the resulting signal observed at the Σ-port is equal to the sum of these signals, whereas at the Δ- port the resulting signal is equal to the difference of these signals.

Mathematica Student Version 2.2 [3] was used to verify the sum and difference action of radiation pattern by plotting various cases as it is shown in Figure 1.3. Figure 1.3(a) is the radiation pattern of a half-wave dipole located at the origin. Figure 1.3(b) is the corresponding sum pattern when both dipoles are excited in equal amplitude and phase. It is obvious from the plot that the radiation pattern is intensified along the y-axis. Difference radiation pattern due to 180° out of phase feed is shown in Figure 1.2 (c), indicating the presence of a null pattern along the y-axis.

1.5 Applications

One of the applications of the zero-sum antenna [4] is shown in Figure 1.4. It is applied to identify the direction of a target. For a single zero-sum antenna, the object can only be identified in only one single angular coordinate which is either an elevation or an azimuth . Here, the application will utilize the elevation direction.

Let V_Σ represents the sum signal and V_Δ be the difference signal. Let V_1 the voltage corresponding lobe 1 and V_2 the voltage corresponding to lobe 2, respectively. The signal received from lobe 1 coverage region then will appear at the input port 1 of the hybrid ring coupler and will be divided into two. One half of the signal will go to the sum port and the

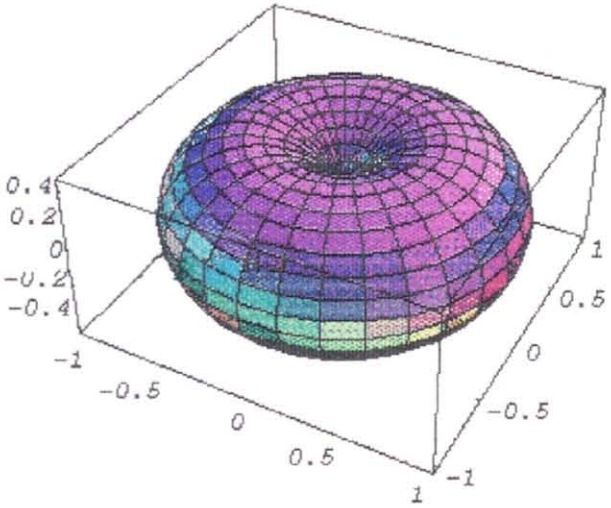

A. Single element radiation pattern

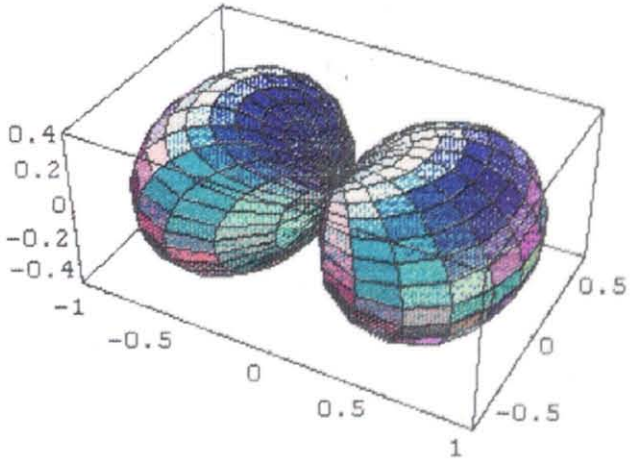

B. Sum radiation pattern

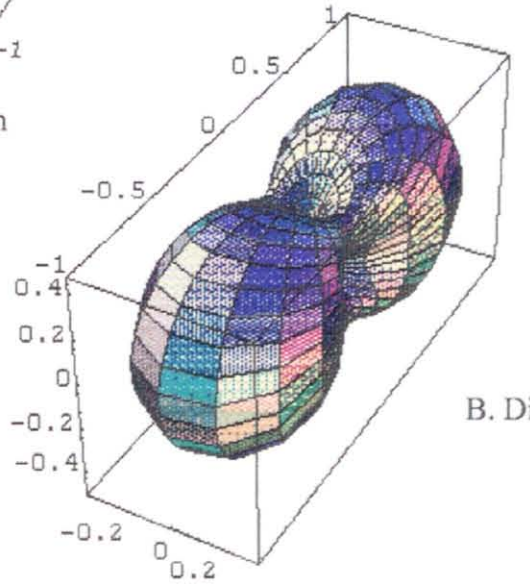

B. Difference radiation pattern

Figure 1.3 Sum and difference radiation pattern of two halfwave dipoles placed half wavelength apart

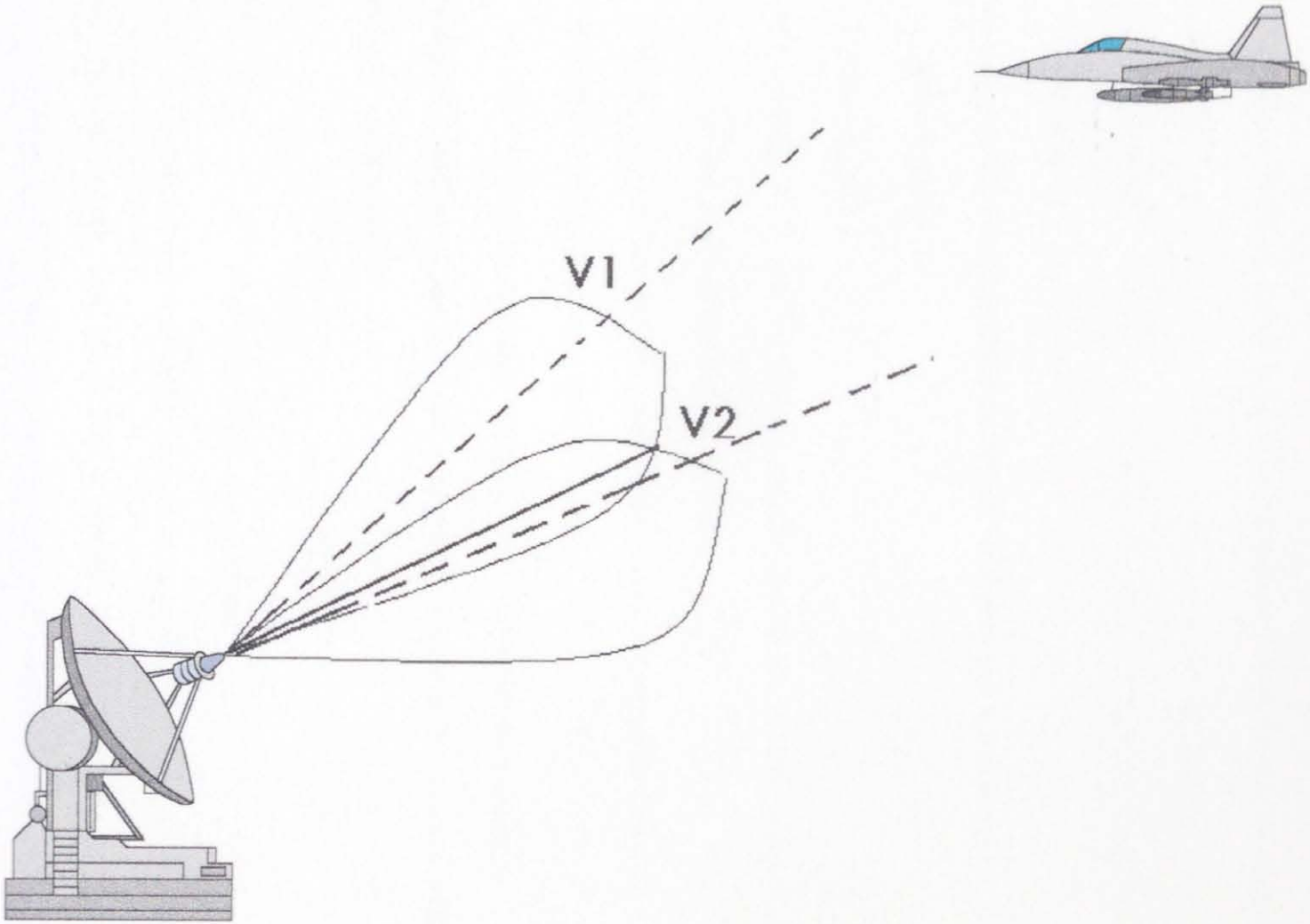

Figure 1.4 Direction finding using zero-sum antenna

other half to the difference port. The signal received due to the lobe 2 coverage region will behave similarly except there will be cancellation due to a 180° phase shift. In terms of the voltages, the half power point is equal to the applied voltage divided by square root of two, therefore:

$$V_{\Sigma}=(V_1+V_2)/\sqrt{2}$$

$$V_{\Delta}=(V_1-V_2)/\sqrt{2}$$

From above equations, we can evaluate the applied voltage at port 1 and port 2 by:

$$V_1=(V_{\Sigma}+V_{\Delta})/\sqrt{2}$$

$$V_2=(V_{\Sigma}-V_{\Delta})/\sqrt{2}$$

With the knowledge of V_1 and V_2, one can identify whether the antenna is aimed at the target, higher than the target, or lower than the target.

If $V_1-V_2 > 0$, then the antenna is directed too high in the elevation direction,

If $V_1-V_2 = 0$, then the antenna is on the target,

If $V_1-V_2 < 0$, then the antenna is directed too low in the elevation direction.

With a digital controller, it can lock into a target by adjusting the antenna until the relation $V_1=V_2$ is satisfied.

1.6 Description of the Thesis

In Chapter 2, the advantages and disadvantages of several electromagnetic simulation methods and an introduction to IE3D, a spatial domain method of moments electromagnetic simulation software which will be used in this work are included.

In Chapters 3 and 4, an application of electromagnetic simulation software to the design and analysis of components of zero-sum antenna, which are the microstrip patch antenna and the stripline hybrid ring coupler are discussed.

In Chapter 5, the integration of both the microstrip path antenna and the stripline hybrid ring directional coupler to form a zero-sum antenna is studied. Experimental results are compared with simulation results.

Finally, conclusions are included in Chapter 6 .

CHAPTER 2

INTRODUCTION TO IE3D; A SPATIAL DOMAIN METHOD OF MOMENTS BASED ELECTROMAGNETIC SIMULATION SOFTWARE

2.1 Comparison Between Several Numerical Analysis Methods

Currently available various commercial electromagnetic simulation software packages are based on numerical methods such as:

-Method of Moments (MoM) in Spectral Domain,

-Method of Moments in Spatial Domain,

-Finite Element Method (FEM),

-Finite Difference Time Domain Method (FDTD) [5], and Transmission Line Matrix Methods (TLM) [6].

Each method has its own advantages as well as disadvantages depending on the particular specifics of the given application. The brief description of each method and its relation to the work done in this thesis are presented below:

1. *Method of Moments in Spectral Domain:* This method has been developed for analysis of structures commonly described as closed problems, i.e. filters, resonators, etc. The antenna problem considered in this work falls into a class commonly described as an open problem requiring the usage of radiation condition. Due to limitation of the spectral domain approach, boundary conditions which require usage of radiation condition are not adequately addressed by this method. Additional inherent disadvantage is due to uniform sampling required through usage of FFT built into this method. Closed structures such as hybrid ring couplers will be modeled inaccurately due to inadequate aspect of the uniform sampling.

2. *Finite Element Method:* The main disadvantages of this method is that it requires exhaustive computational effort (number crunching) as well as extensive RAM requirements. As a result, it takes a long time to compute structures of even moderate size. However it does not encounter limitation in terms of geometrical shape constraints. In the future when computer speed and RAM will not be of a concern, then FEM may become an attractive method for electromagnetic simulation. Recent efforts in extending FEM into time domain may lead to a new possibility if the above mentioned difficulties are alleviated.
3. *Finite Difference Time Domain (FDTD) and Transmission Line Matrix (TLM) methods* : both methods have similar difficulties. They require solution of both magnetic and electric fields in three dimensional space, therefore, the number of unknown variables increase significantly. They need uniform griding, extensive computer power and memory, and therefore it takes a long time to complete the desired simulation. The most outstanding features of both methods is that they are simple to be programmed and they produce results in time domain directly. It needs only one execution in time which can offer a corresponding wideband frequency response. Additional attractiveness in FDTD is its usage in conjunction with circuit simulators, since it has the ability to handle lumped components effectively.
4. *Method of Moments in Spatial Domain Method:* It is an open boundary simulator. It uses both rectangular and triangular cells, therefore, it has a capability to simulate arbitrary shapes. The main attractive feature of this approach is that it requires solution of the current distribution on the conductors only in the 3-D, multi-layered sections, therefore it takes a lot less time than FEM, FDTD, & TLM. Therefore, it is

the most suitable software due to its capabilities and its efficiency to be used in the current application with available limited computer resources.

2.2 Introduction to IE3D

The emerging electromagnetic simulation tools in microwave/millimeter-waves engineering are forming backbone for the successful fabrication of complicated high density circuits built as microwave monolithic integrated circuits (MMIC) chips for applications in transmitters, receivers, amplifiers, phase detectors, etc.

The three most basic transmission lines employed in the MMIC technology are microstrip, slotted-line, and co-planar waveguides, which all can be classified as planar structures. In the past, the dominant transmission guides were either heavy and bulky rectangular, cylindrical hollow metallic waveguides or coaxial cables. Unlike conventional classical waveguide structures, exact analytical analysis of open guided quasi-TEM mode and higher order modes is not available, therefore numerical analysis is the only means in attempting to solve these complicated issues.

IE3D [6] is based upon a full-wave integral equation, solved by method of moments. Current distributions on a true 3-D, multi-layered metallic structures of arbitrary shapes are determined as an outcome of these simulations. In the IE3D software tool, currents on true 3-D metalization can be modeled at any arbitrary angle. It automatically discretizes regular region with rectangular cells and irregular region with triangular cells. Rectangular cells yield faster solutions whereas triangular cells require longer computational time. With this automatic mixed meshing rectangular and triangular cells capability, IE3D provides nearly optimum solutions for arbitrary shape structures.

IE3D has a total of three modules: MGRID, MODUA, and CURVIEW. MGRID is a Windows 95 or Windows NT graphical layout editor. MODUA is a post-processor for calculating S-parameters and impedance. CURVIEW is also a post-processing tool capable of determining current distributions, current distribution vectors, and 3-D radiation patterns.

One of the best features of the IE3D is its built-in gradient optimization routine which is especially valuable in this application in determining the resonant length of the patch, as well as the location of the feed probe. Because the location of the probe has an effect on both input impedance and resonant frequency of the antenna, it is very difficult simultaneously to place the probe where one can match the antenna and also optimize the antenna size for the desired resonant frequency. With such built-in optimization in IE3D, the user can optimize simultaneously the optimum feed point location as well as the desired resonant frequency dimension.

Scalar and vector current distributions are also very important features which help the user to be able to visualize where current heavily concentrates and in which direction the current flows in the given geometry. True 3-D radiation pattern, mapped 3-D radiation patterns, polar and rectangular display of 2-D patterns, gain, directivity, all are evaluated and are provided as output parameters. All these features are very practical as trouble shooting tools for the analysis and design of general radiating structures.

CHAPTER 3

MICROSTRIP PATCH ANTENNA

3.1 Introduction

Low profile, light weight, ease in fabrication, rugged, conformal, and in some cases lower cost than comparable antennas, are among favorable features which help microstrip antenna to be used in a broad range of applications. Microstrip antennas have been designed and incorporated in very wide range of systems; from commercial car navigation systems, biomedical systems, intruder alarms, to sophisticated satellite communication systems, on board ship radars, etc.

The basic microstrip resonator [8] geometry given in Figure 3.1 consists of a dielectric sheet of thickness h and relative dielectric constant ε_r. The finite conductor with a variety of shapes is deposited on the top of the dielectric helps the whole structure to radiate.

3.2 Microstrip Resonator Classification

The microstrip radiator can be classified into two categories. The narrow strip resonator is usually called the microstrip dipole antenna whereas the broader conductor is known as a microstrip patch antenna. Figure 3.1 illustrates various shapes of microstrip patch antennas and a dipole microstrip antenna.

3.21 Microstrip Dipole

The small size of the microstrip dipole antenna makes it very attractive for many applications. Due to the width much smaller compared to the length, there is no transverse current flow on it, therefore cross polarization level is inherently low. However this condition also leads to a very narrow bandwidth.

3.22 Microstrip Patch Antenna

Microstrip patch antenna may have varieties of shapes; rectangular, square, circular, ring, triangular, or elliptical as shown in Figure 3.1. The selection of a particular shape depends on the parameters one wishes to optimize: e.g. antenna size, sidelobes, cross polarization, and impedance bandwidth, etc.

Because of the broader width, microstrip patch antenna may excite surface current flowing across the transverse direction which will in turn create unwanted cross polarization radiation interference effects. The intensity of this undesired radiation depends strongly on the feeding methods and location of the feed.

3.3 Analytical Models for Rectangular Patch Antenna

Although the geometry of a rectangular microstrip antenna appears to be simple, it becomes quite difficult to determine the electromagnetic field effects analytically due to the presence of complex boundary conditions at the interface between dielectric substrate, metal, and air. For accurate analysis, full-wave electromagnetic solver is employed. In this work, as an example, IE3D will be used to analyze and design a single element microstrip patch antenna at f=2.254 GHz.

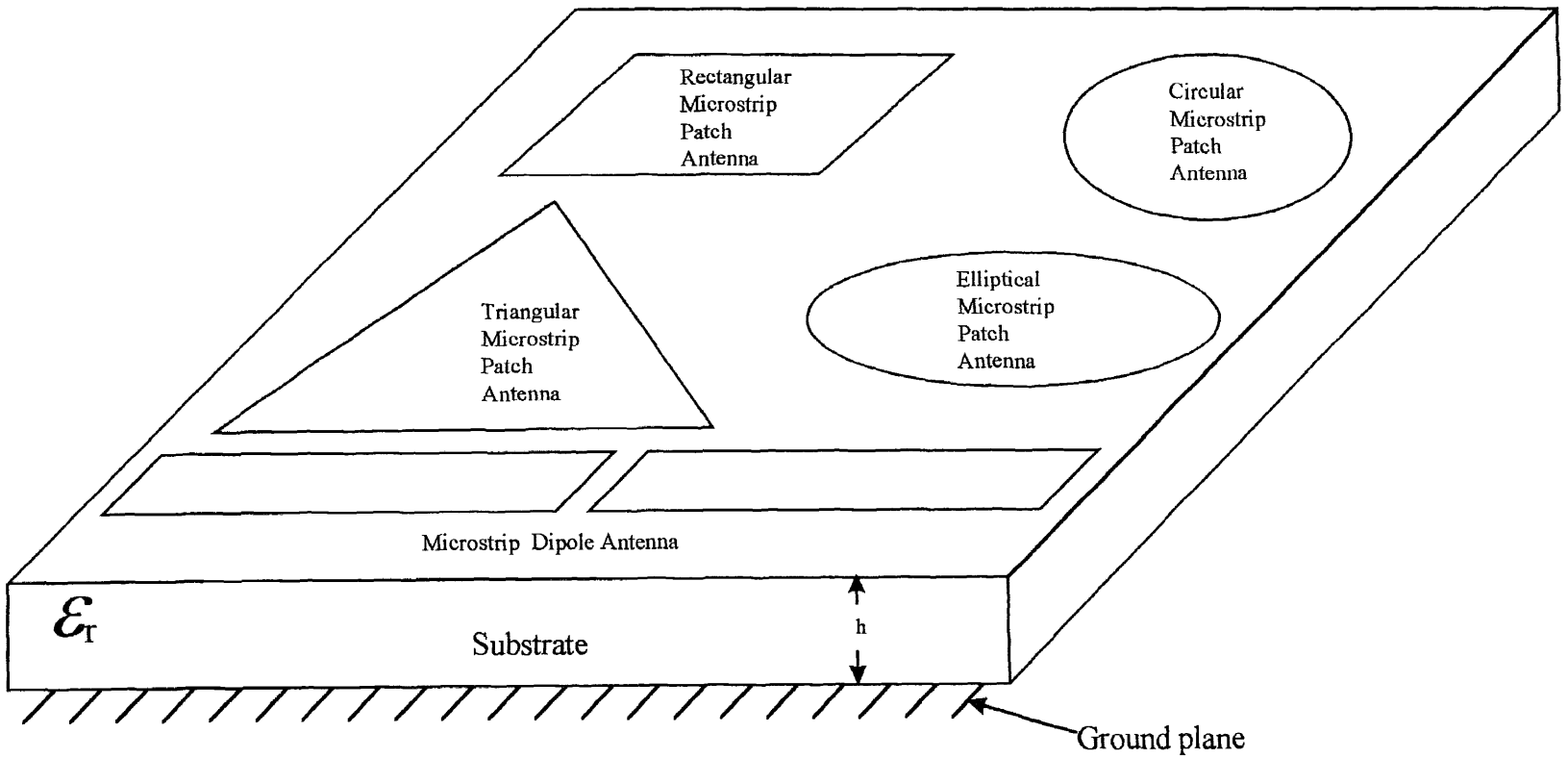

Figure 3.1 Various shaped microstrip patch antennas

Even though, one can obtain very accurate results for patch radiation using simulation tools, one may not be able to gain directly valuable insight on how it actually radiates. Simple approximate analytical models help to fill in such gaps. The popular analytical models are based on an equivalent transmission line model and a cavity model. A combination of both simplified models and accurate numerical analysis results will offer the maximum insight on how such a structure radiates.

3.31 Transmission Line Model

Transmission line model [7] is the simplest of all approximate methods. It utilizes transmission line theory to model the patch in terms of parallel radiating slots as shown in Figure 3.2. Each radiating slot has a width w and a height h. Because of its simplicity, it does not provide accurate results, however, it does suggest some physical insights on how energy radiates into upper half space. But it does not predict the presence of higher order modes. The more complicated cavity model can predict the existence of higher modes, however it does not give any clues on equivalent sources which are responsible for the radiation.

A. *Microstrip transmission line*

A microstrip line consists of a strip conductor and a ground plane separated by a dielectric substrate as shown in Figure 3.3. Both electric and magnetic fields are not confined entirely within the substrate below the conducting patch but partial fringing fields also exists in air so the propagation of electromagnetic energy in the microstrip line is not restricted to a pure transverse electromagnetic (TEM) mode but necessitates inclusion of

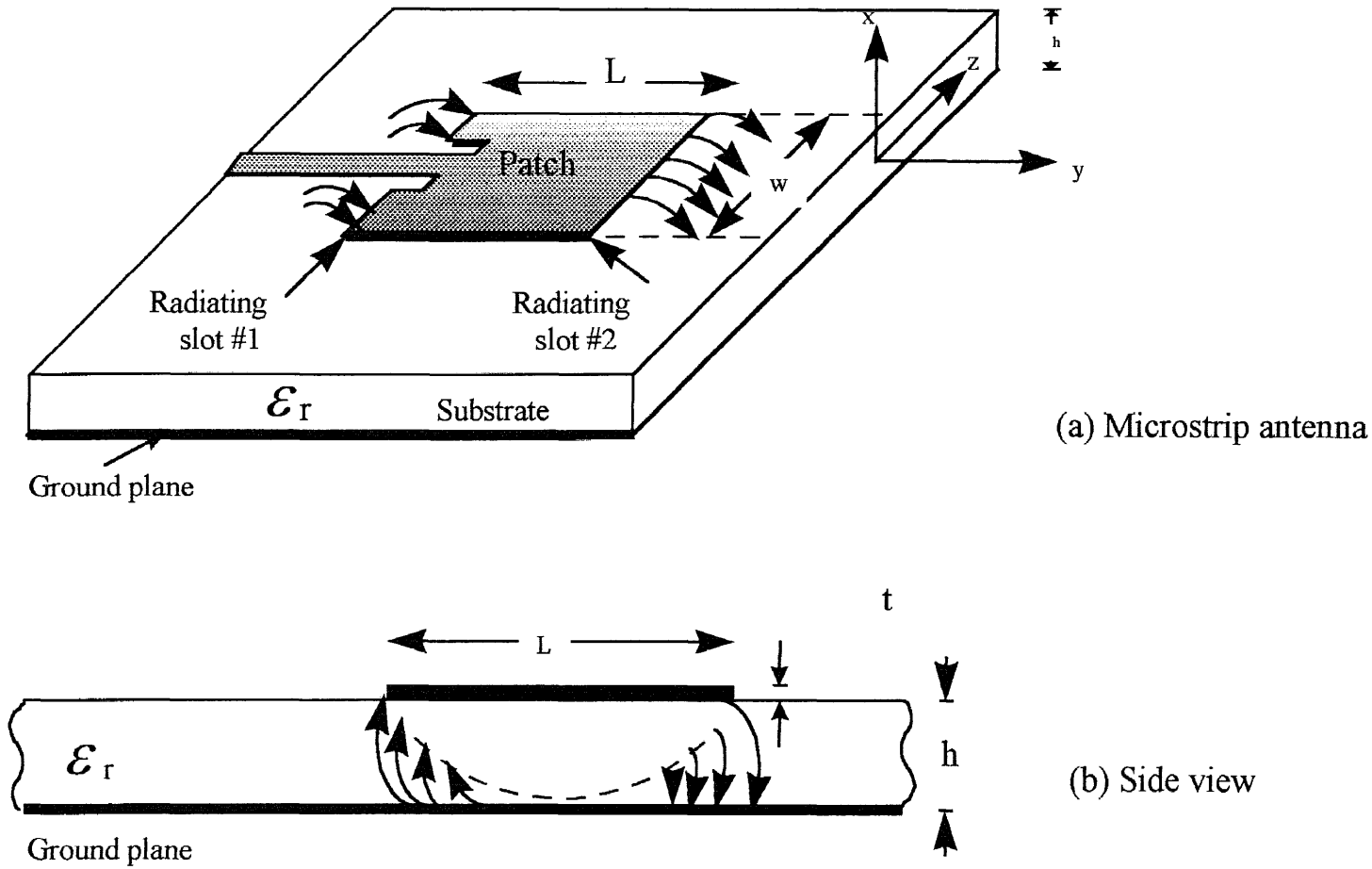

Figure 3.2 Microstrip antenna and its equivalent transmission line model [8].

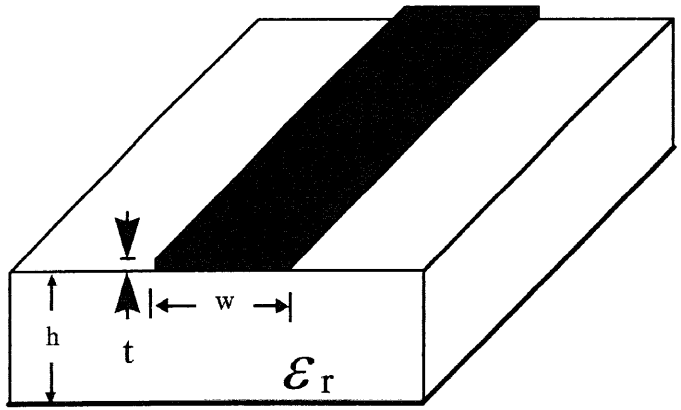

(a) Microstrip line

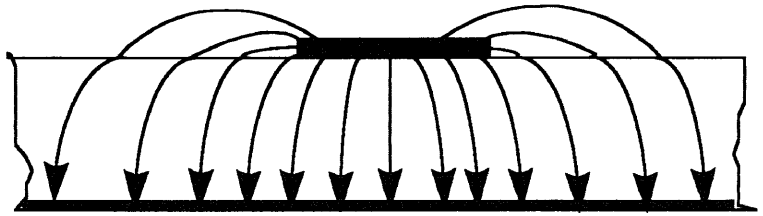

(b) Electric field and fringing field

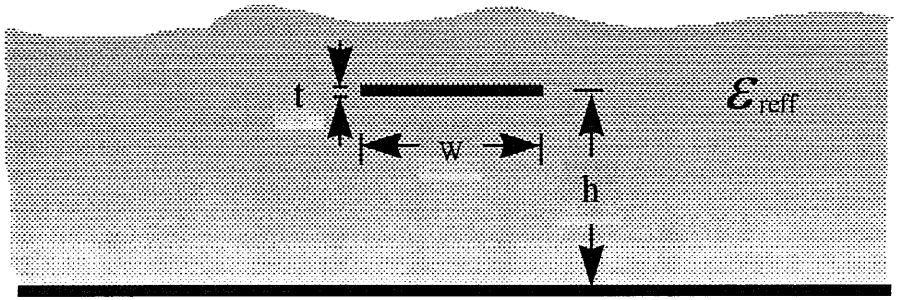

(c) Effective dieclectric constant

Figure 3.3 Microstrip line and effective dielectric constant [8].

a quasi-TEM mode as well. The characteristic impedance of the microstrip line can be expressed as [9]

$$Z_0 = \frac{60}{\sqrt{\varepsilon_{r,eff}}} \cdot \ln\left[\frac{8}{\left(\frac{w}{h}\right)} + 0.25 \cdot \frac{w}{h}\right] \quad \text{for} \quad \frac{w}{w} \le 1$$

$$Z_0 = \frac{\frac{120\pi}{\sqrt{\varepsilon_{r,eff}}}}{\left(\frac{w}{h} + 1.393 + 0.667\ln\left(\frac{w}{h} + 1.444\right)\right)} \quad \text{for} \quad \frac{w}{h} \ge 1$$

B. *Effective dielectric constant.*

With finite line width, the fields at the edge undergo fringing and make the microstrip appear like wider electrically compared to its actual physical dimension. Effective dielectric $\varepsilon_{r,eff}$ is introduced to account for both fringing and the presence of a quasi-TEM mode. Effective relative dielectric constant is defined as the relative dielectric constant of the corresponding uniform dielectric material so that the electrical characteristics of the structure in Figure 3.3(b) is same as in Figure 3.3(c) especially in terms of the propagation constant.

The effective dielectric constant of a microstrip line is a function of the dielectric constant ε_r, the height h of the dielectric substrate, and the width w of the strip conductor. The effective relative dielectric constant is given by [10]:

If $t/h << 0.005$:

$$\varepsilon_{r,eff} = \frac{\varepsilon_r + 1}{2} + \frac{\varepsilon_r - 1}{2} \cdot \left[\left[1 + \frac{12}{\left(\frac{w}{h}\right)} \right]^{-\frac{1}{2}} + 0.04 \cdot \left(1 - \frac{w}{h} \right)^2 \right] \quad \text{for } \frac{w}{h} \le 1$$

$$\varepsilon_{r,eff} = \frac{\varepsilon_r + 1}{2} + \frac{\varepsilon_r - 1}{2} \cdot \left[1 + \frac{12}{\left(\frac{w}{h}\right)} \right]^{-\frac{1}{2}} \quad \text{for } \frac{w}{h} \ge 1$$

C. *Effective length, effective width, and resonant frequency*

Because of the fringing field effects on the radiating edge of the microstrip patch antenna, its effective length will be longer than its physical dimension as shown in Figure 3.4. Its length is extended by an additional amount of Δl on both ends of the radiating edge and expressed as [11]

$$\frac{\Delta L}{h} = 0.412 \left(\frac{\varepsilon_{r,eff} + 0.3}{\varepsilon_{r,eff} - 0.258} \right) \cdot \left[\frac{\frac{w}{h} + 0.264}{\left(\frac{w}{h} + 0.8\right)} \right]$$

Since additional length $2\Delta l$ added into the total length L, the effective length of this patch will be $L_{eff} = L + 2\Delta l$.

The resonant frequency of the patch antenna is given by

$$f_r = \frac{1}{2L \cdot \sqrt{\varepsilon_r} \cdot \sqrt{\mu_0 \cdot \varepsilon_0}} = \frac{c}{2L \cdot \sqrt{\varepsilon_r}}$$

where c is the velocity of light in vacuum. Above formula did not take into account the modified value of the effective length. Therefore, a more accurate version of resonant frequency for the patch can be expressed as [8]:

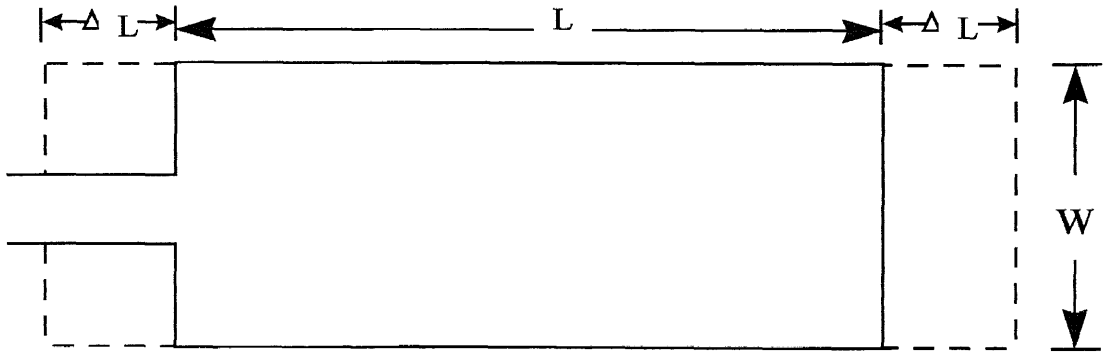

(a) Top view

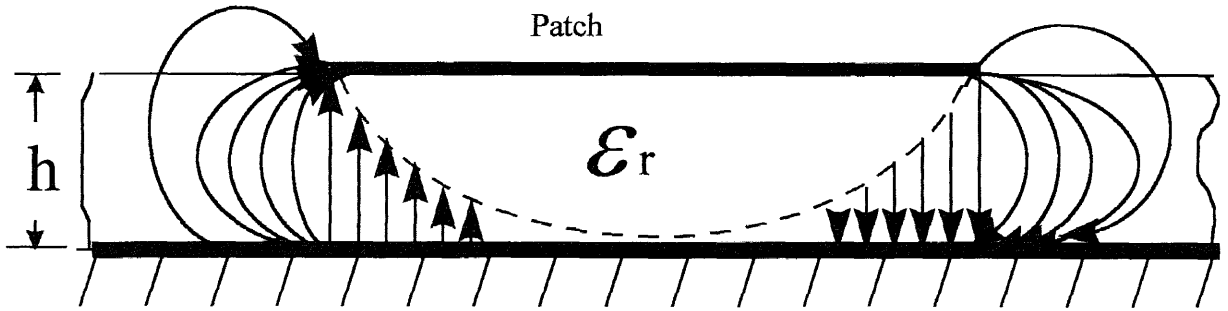

(b) Side view

Figure 3.4 Physical and effective length of rectangular microstrip patch [8].

$$f_{r,eff} = \left(q \cdot \frac{1}{2L \cdot \sqrt{\varepsilon_e} \cdot \sqrt{\mu_0 \cdot \varepsilon_0}} \right) = \left(q \cdot \frac{c}{2L \cdot \sqrt{\varepsilon_r}} \right) = q \cdot f_r$$

$$q = \frac{f_{r,eff}}{f_r}$$

where q is defined as the fringing factor or length reduction factor.

From transmission line model, one can estimate the resonant frequency of the rectangular patch microstrip antenna. When the substrate height increases, extended fringing causes Δl to expand which forces the decrease in the resonant frequency.

3.32 Cavity Models

Cavity model is more complex in nature in comparison to the transmission line model. Here, the rectangular microstrip patch is modeled as a dielectric loaded cavity where the normalized field within the dielectric substrate can be calculated accurately by assuming that region as a cavity bounded by the patch and the bottom ground plane (perfect conducting electric walls) with perfect conducting magnetic wall in surrounding perimeter of the patch as shown in Figure 3.5. Cavity model has the ability to predict higher order modes supported by the structure and the corresponding resonant frequencies for the cavity are given as [12, 13]:

$$\left(f_{r,eff}\right)_{mnp} = \frac{1}{2\sqrt{p \cdot \sqrt{\mu\varepsilon}}} \cdot \sqrt{\left(\frac{m\pi}{h}\right)^2 + \left(\frac{n\pi}{L}\right)^2 + \left(\frac{p\pi}{w}\right)^2}$$

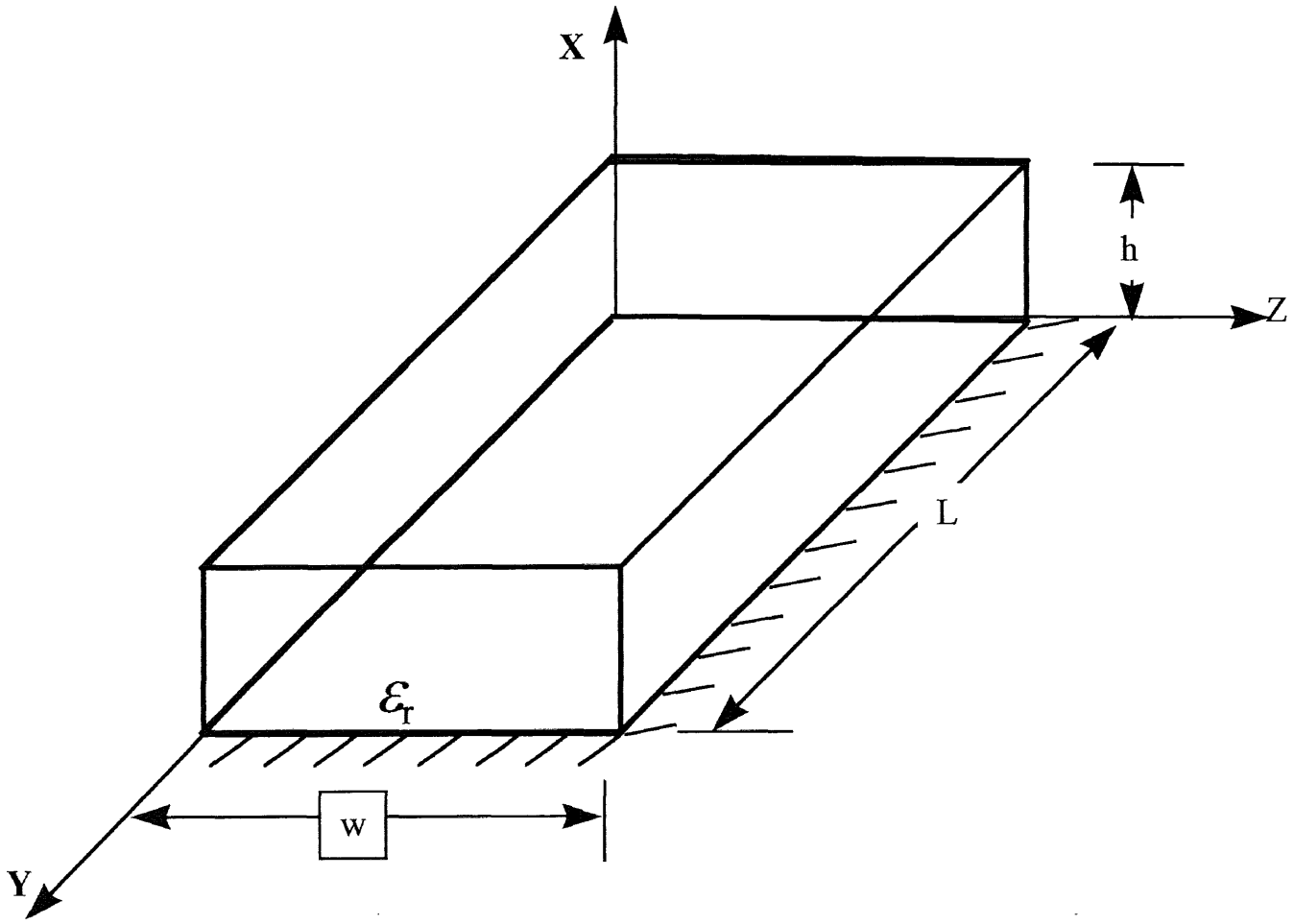

Figure 3.5 Rectangular microstrip patch geometry for a cavity model [8]

where m,n,p represent the number of half-cycle field variations along the x,y,z directions respectively. Figure 3.6 shows the field configurations for the dominant and the first three higher order modes.

A. *Radiation patterns of a rectangular microstrip patch antenna*

The approximate far field radiation patterns of a rectangular microstrip antenna operating in the dominant mode in both E and H planes, respectively are given by [8]:

E-plane ($\theta = \pi/2$):

$$\varepsilon_\phi = -j \cdot \frac{2k_0 \cdot wv_0 \cdot e^{-jk_0 \cdot r}}{\pi r} \cdot \left[\frac{\sin\left(\frac{k_0 \cdot h}{2} \cdot \cos\phi\right)}{\left(\frac{k_0 \cdot h}{2}\right) \cdot \cos\phi} \right] \cdot \cos\left(\frac{k_0 \cdot L_e}{2} \cdot \sin\phi\right)$$

and H-plane ($\phi = 0$)

$$\varepsilon_\phi = -j \cdot \frac{2k_0 \cdot wv_0 \cdot e^{-jk_0 \cdot r}}{\pi r} \cdot \sin\theta \cdot \frac{\sin\left(\frac{k_0 \cdot h}{2} \cdot \sin\theta\right) \cdot \sin\left(\frac{k_0 \cdot w}{2} \cdot \cos\theta\right)}{\left(\frac{k_0 \cdot h}{2}\right) \cdot \sin\theta \cdot \frac{k_0 \cdot w}{2} \cdot \cos\theta}$$

3.4 Antenna Feeds

Coaxial feed (probe feed), direct microstrip (inset and non-radiating) feed, proximity feed, and aperture coupled feed could be considered among the most popular feed structures utilized in microstrip antennas.

Coaxial feed is widely used as a microstrip feed due to its ease in fabrication. The probe extends from underneath the ground plane, penetrates through the substrate, and is

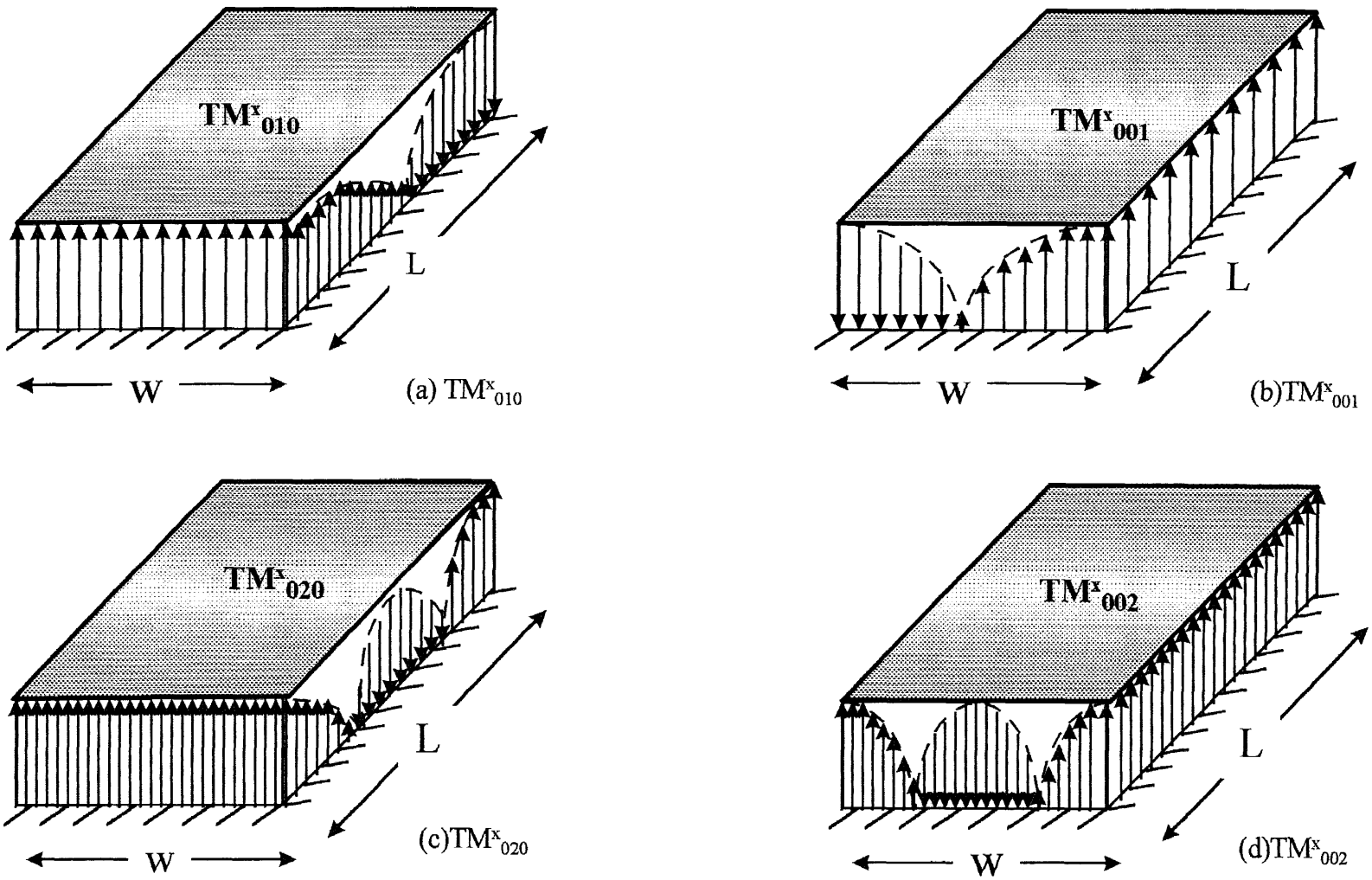

Figure 3.6 Field configurations (modes) for a rectangular microstrip patch [8].

connected to the patch. It is totally hidden under the big patch therefore theoretically generates no spurious radiation. Figures 3.7, 3.8, and 3.9 were generated using IE3D where simulations showed the different vector current distributions due to coaxial feed, microstrip line direct feed on the non-radiating edge, and the inset feed, whereas Figure 3.10, 3.11, and 3.12 illustrate corresponding 3-D radiation pattern plots and corresponding radiation parameters, respectively.

Careful observation of Figure 3.7 reveals no presence of a significant transverse current flow along the non-radiating edges. However, there is a current flow across the transverse direction as shown in Figure 3.8 due to edge coupled feed. This will cause undesired cross polarization as seen in radiation parameters of Figure 3.11. Based on such observation, one can conclude with evidence from Figure 3.10 to Figure 3.12 that coaxial probe feed and inset feed are more desirable than non-radiating edge feed. If the system requires planar structure topology than the inset feed is more preferable. In this work, there is no special requirement on the feeding method, therefore, probe feed can be considered as a suitable alternative.

3.5 CAD Design and Analysis of a Rectangular Microstrip Patch Antenna

In order to facilitate the design process, with the help of simplified models, initial values for resonant frequency and the feed location can be estimated. Approximate results provide good initial values for further optimization.

The calculated dimensions and the feed point location are entered through MGRID which is a Windows 95 graphical interface circuit layout editor of IE3D package. The first run

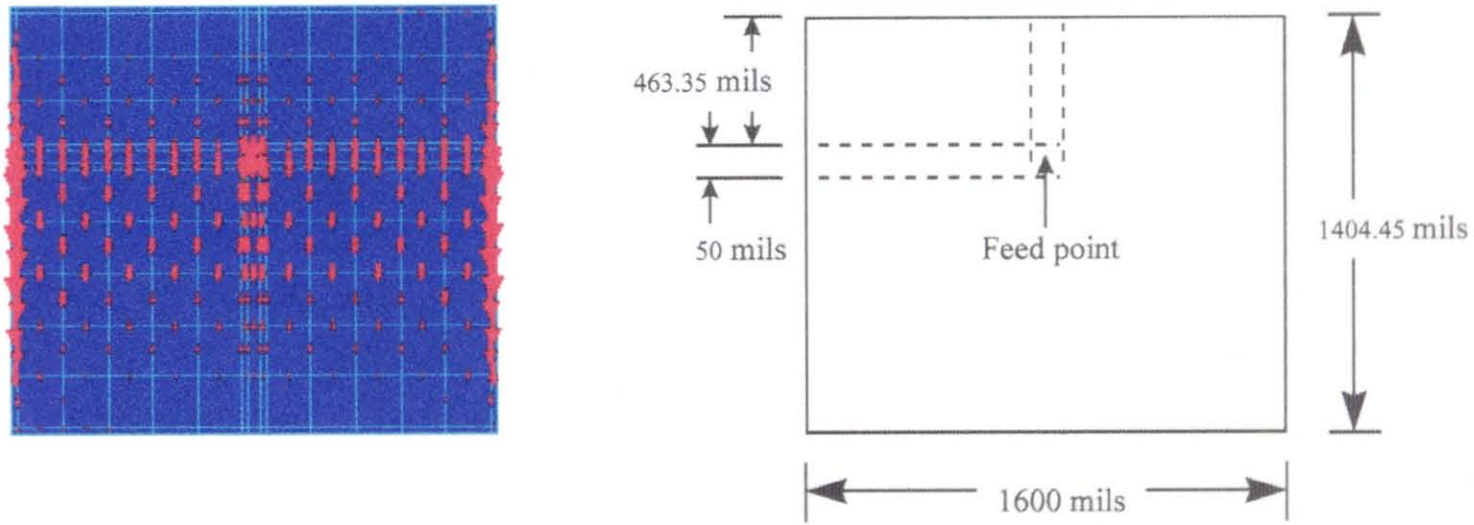

Figure 3.7 Current vector distribution and physical dimension of the single patch attenna

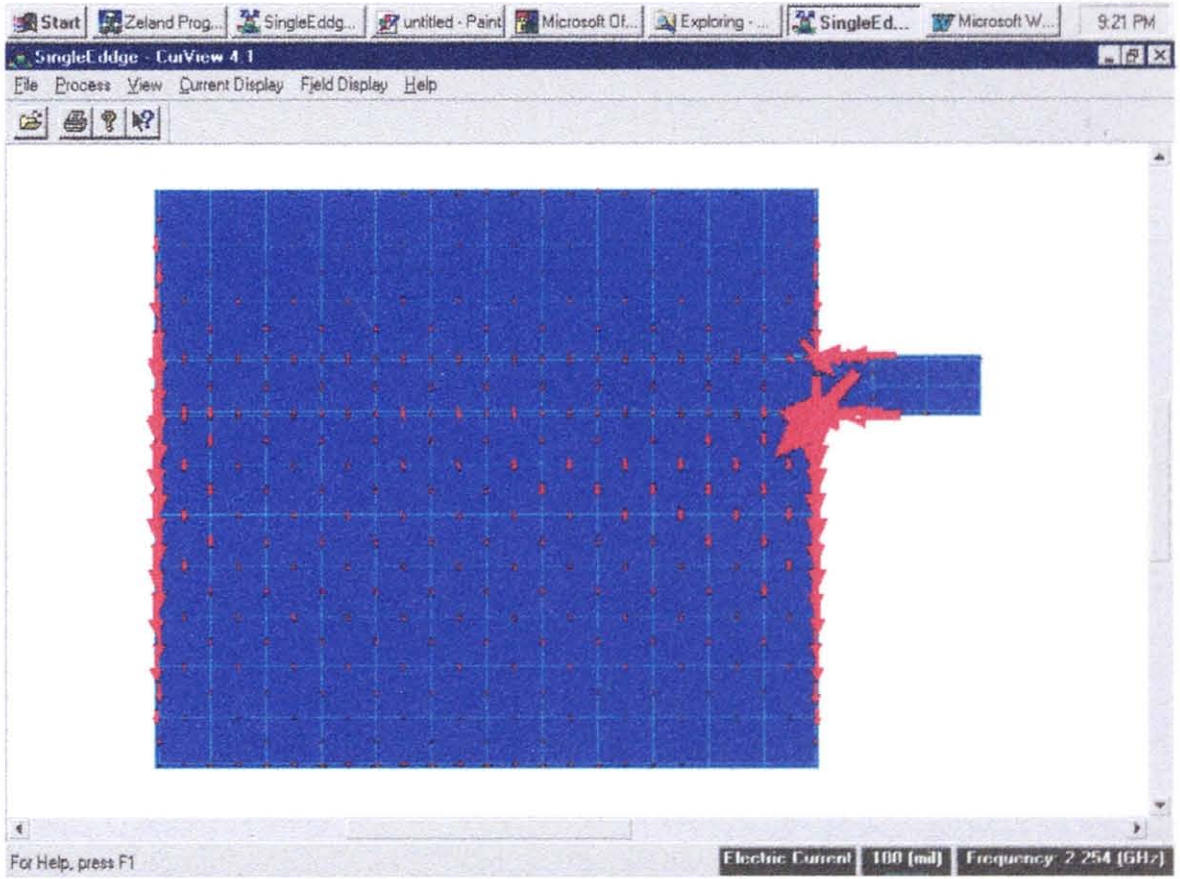

Figure 3.8 Vector current distribution due to microstrip line edge feed of a microstrip patch using ie3d simulation

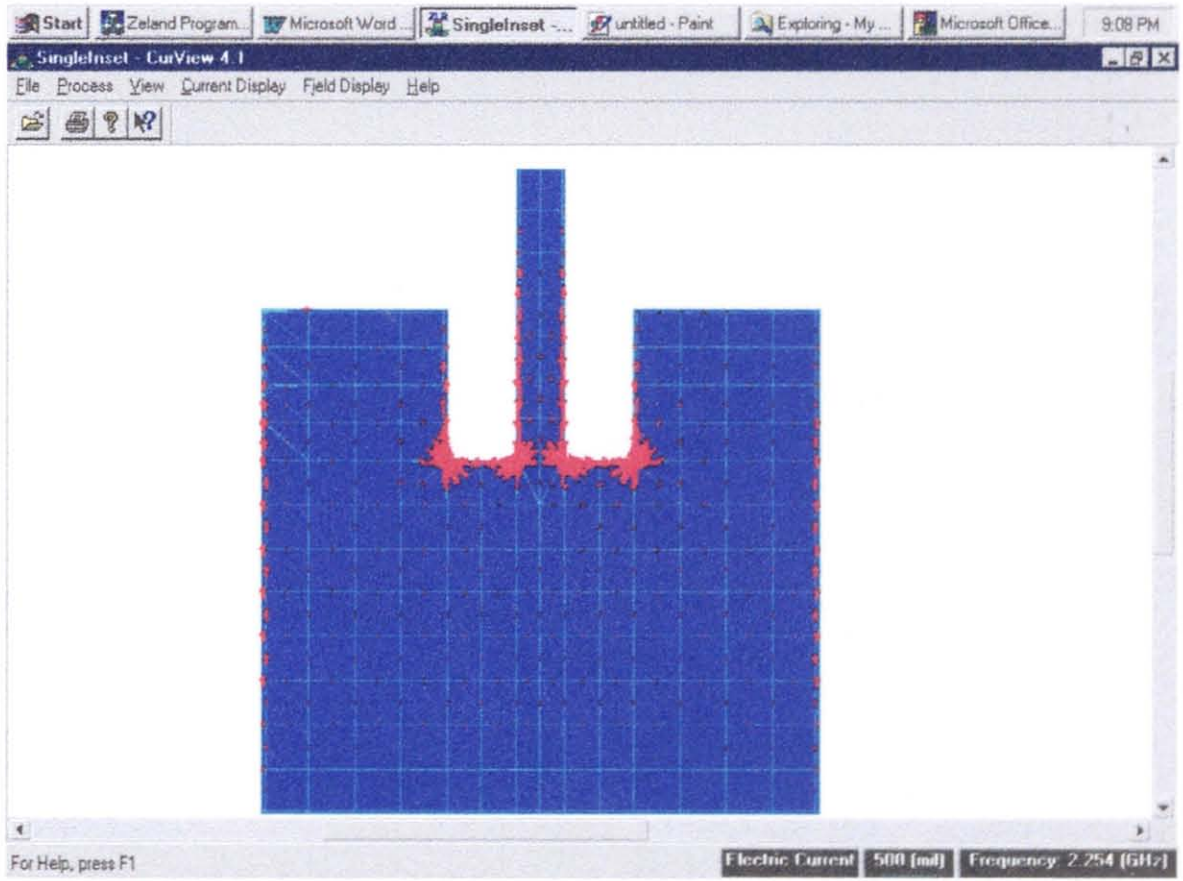

Figure 3.9 Vector current distribution due to microstrip inset feed of a microstrip patch using ie3d simulation

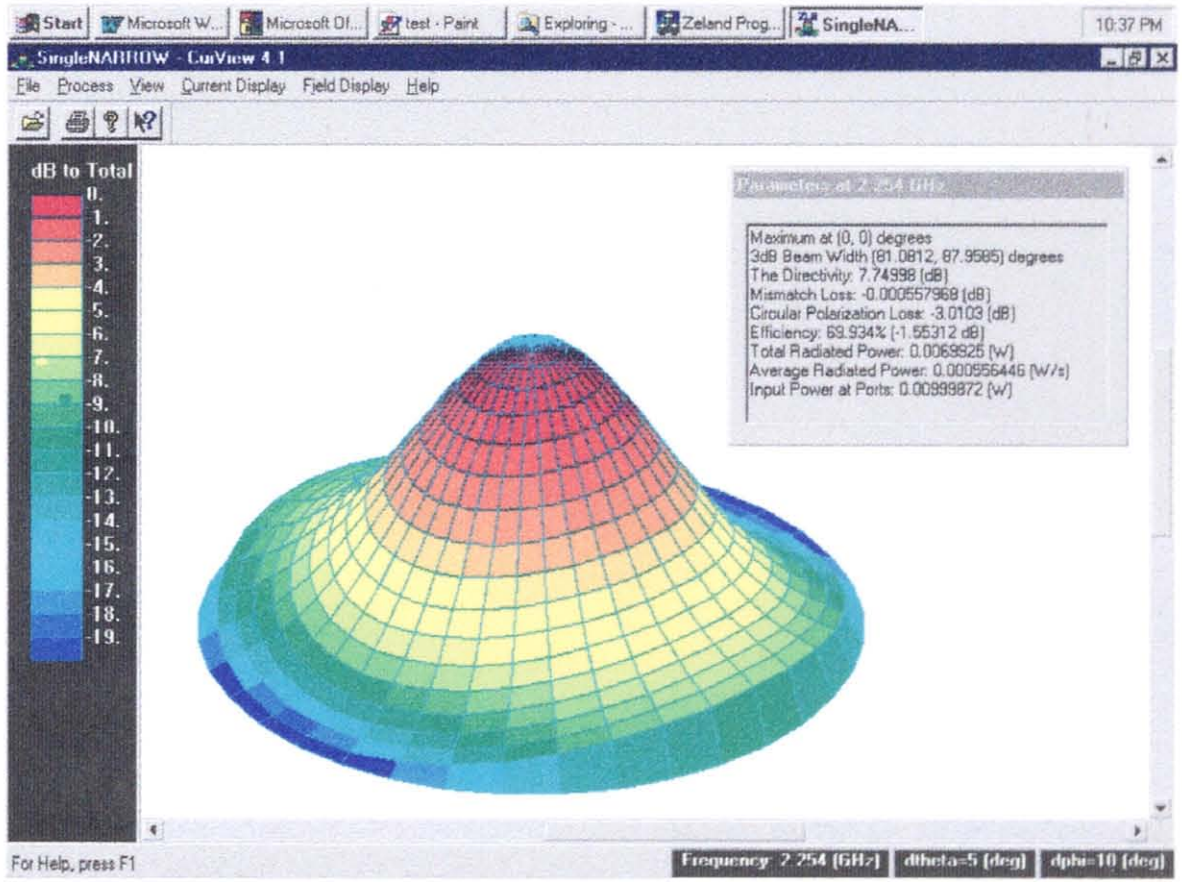

Figure 3.10 Radiation pattern and corresponding radiation parameters due to a probe feed rectangular patch antenna

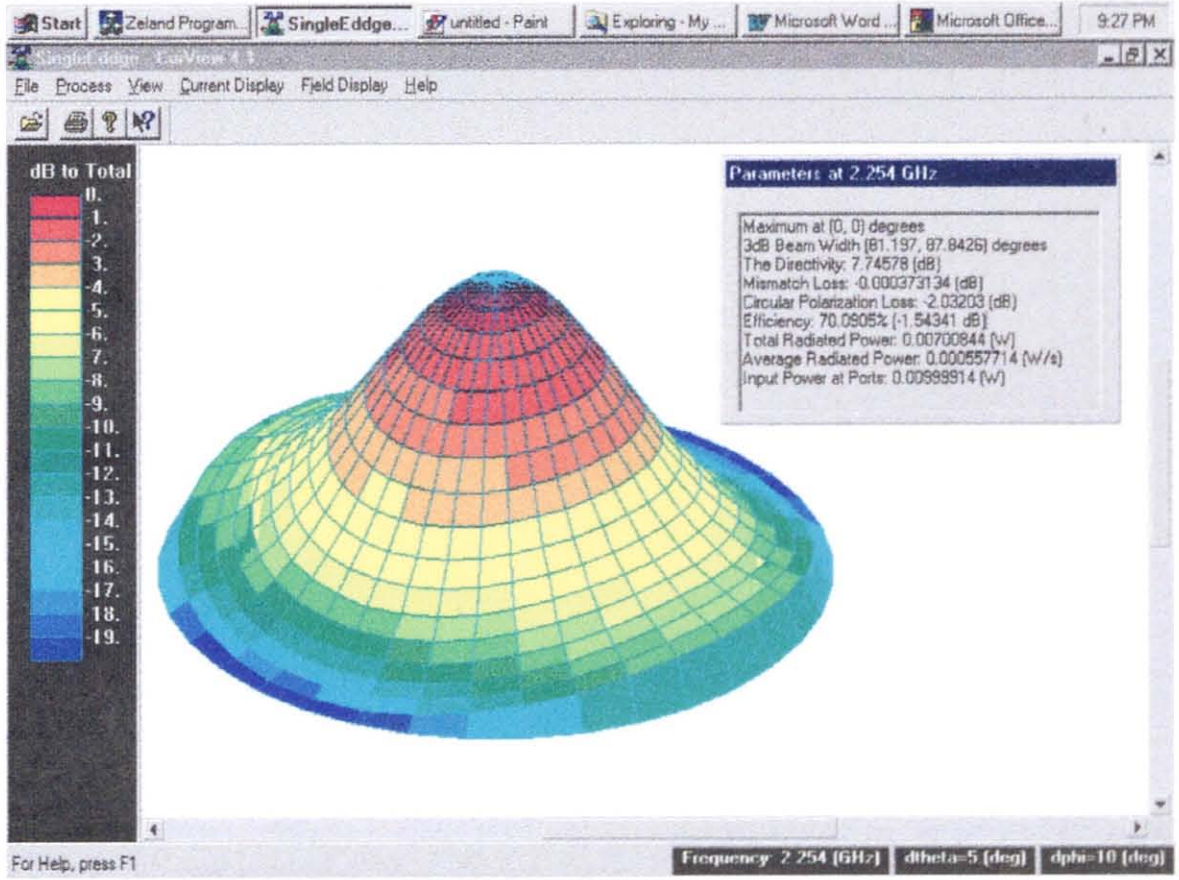

Figure 3.11 Radiation pattern and corresponding radiation parameters due to an edge feed rectangular patch antenna

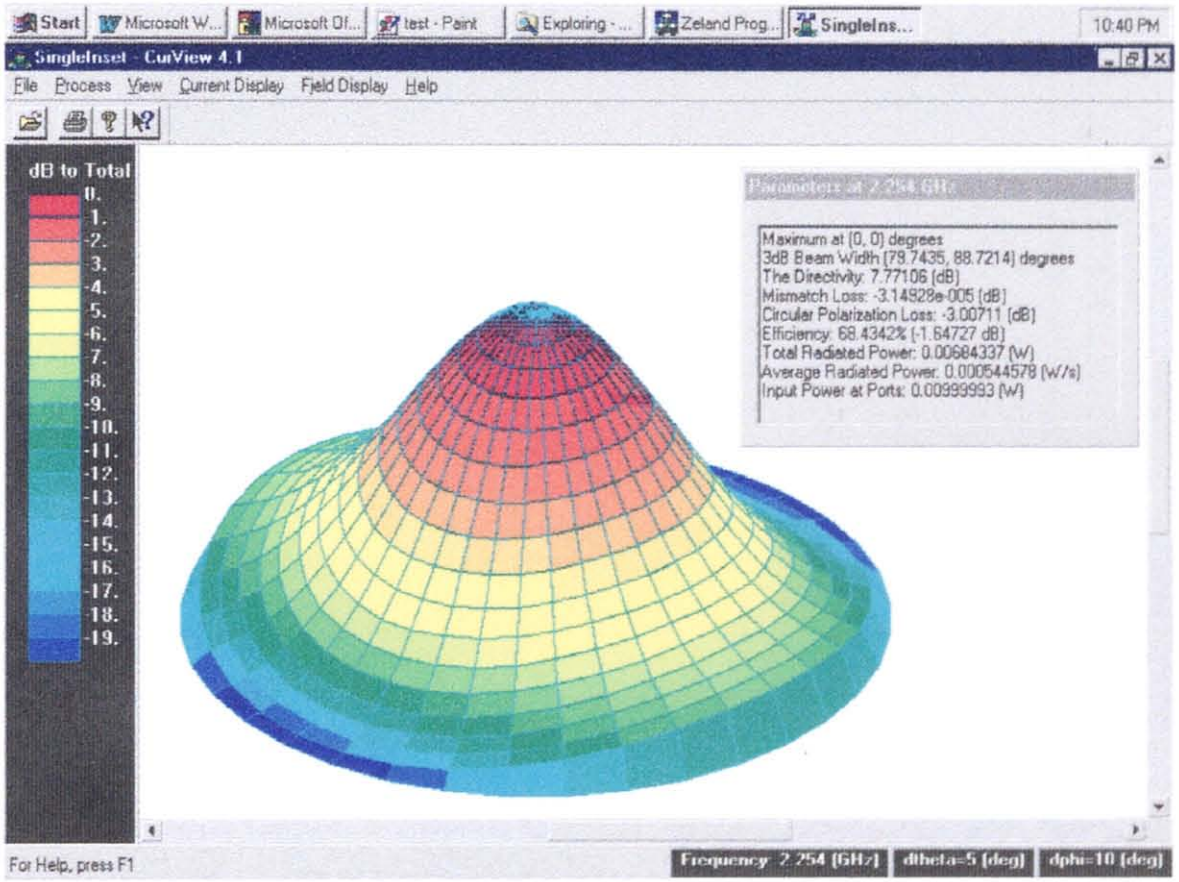

Figure 3.12 Radiation pattern and corresponding radiation parameters due to an inset feed rectangular patch antenna

simulated results are analyzed to identify where resonant frequency shift is and also helps to determine the nature of the impedance of the antenna at the chosen feed location.

A. *Resonant frequency of the patch*

The resonant frequency is determined through the zero cross over of the imaginary part of the impedance. The desired requirement necessitates that for maximum radiation, the antenna impedance should be purely resistive and the radiation resistance should be equal to the generator's impedance to ensure maximum power transfer. If there is cancellation of reactive components in terms of either capacitive or inductive reactances, the net energy storage will not take place and all resistive power left after experiencing possible losses will radiate.

B. *Search for the matched feed location*

The proper feed location is determined by observing the impedance of the antenna at the resonant frequency. Figure 3.13 shows the current density distribution of the patch. One can easily observe that the current is minimum at the edge and maximum in the middle of the non-radiating edge, therefore the impedance is minimum at the center and maximum at the edge. With this information one can immediately predict whether the feed location should be moved forward or backward, accordingly.

C. *Simultaneous optimization for the resonant frequency and the matched feed*

When the probe is moved to a new location, the resonant frequency will be affected due to the interaction of the impedance of the probe with the patch. Adjusting the length of the patch for changing resonant frequency also changes the impedance of the antenna. The total length adjustment leads to the changes in a current density distribution at that location, resulting in modification of the impedance of the antenna.

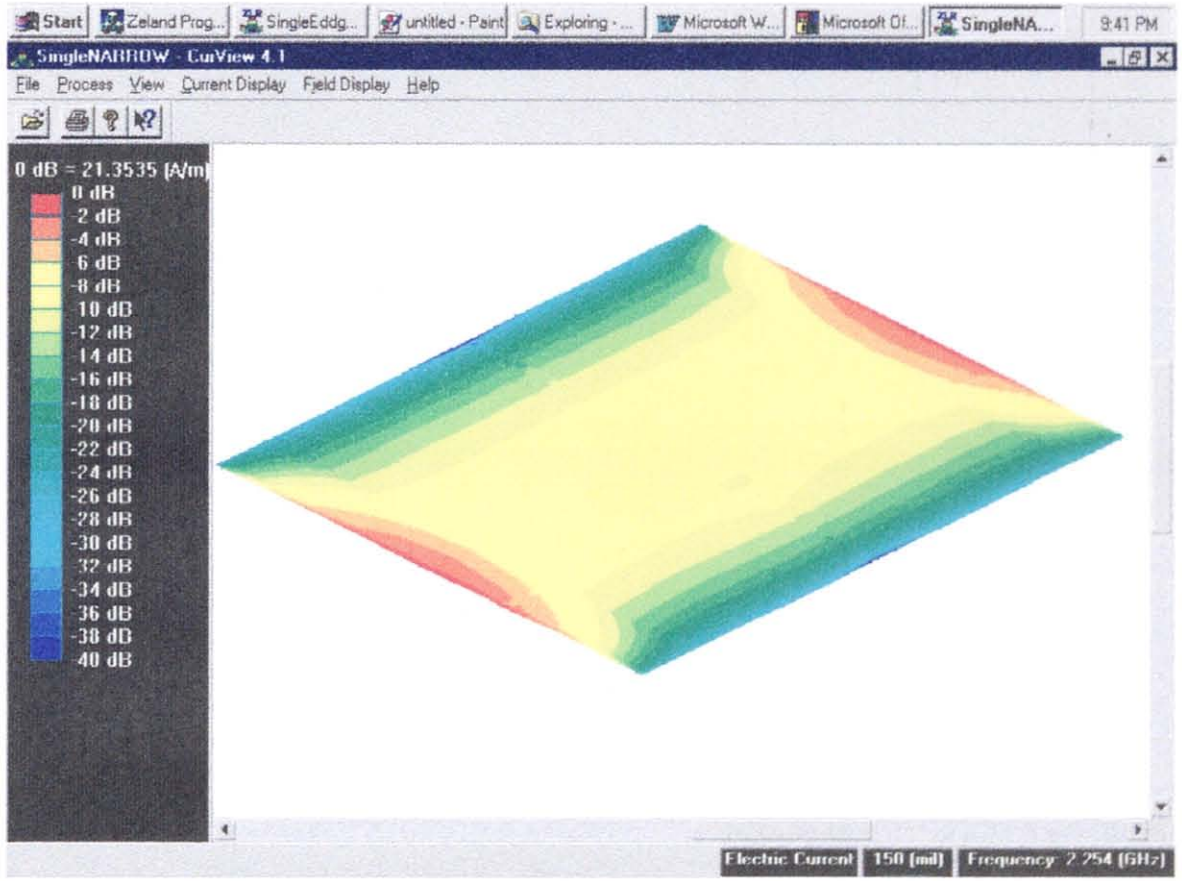

Figure 3.13 Current density distribution of single patch probe feed antenna of Figure 3.7

Most optimization schemes are based on a linear optimization requiring the user to define the solution of the problem as close to the optimum as possible, otherwise iterative solution may be locked into to the local minimum, preventing the proper convergence for the final solution.

As in the case of the patch antenna analyzed here, the user must be able to tune the antenna to the closest possible length and identify the proper feed location. Then, these solutions should be placed into the geometry file for final optimization. The obtained optimized results were quite impressive, most of the time very good return loss can be achieved somewhere between -50 to -60 dB for a single patch antenna as seen in Figure 3.14. This result could be hardly obtained without the help of the built-in optimization routine in IE3D.

Since the cavity model predicts the presence of higher order modes, the resonance frequencies corresponding to these modes are shown in Figure 3.15. The current distributions associated with these higher order modes are depicted in Figures 3.16, 3.17 and 3.18. These current distributions follow the multimode current patterns as are predicted from the equivalent cavity models. The 3-D far-field patterns due to these higher order modes are included in Figure 3.19, 3.20, and 3.21. These patterns have distinct characteristics of far-fields which could have been obtained by using Fourier Transform of the equivalent near fields represented partially in Figure 3.16, 3.17 and 3.18. However, for practical application, polar radiation patterns are adequate to quantify the performance characteristics of these antennas. Figure 3.22 exhibits typical E-plane and H-plane patterns corresponding to the fundamental mode resonating at $f = 2.254$ GHz.

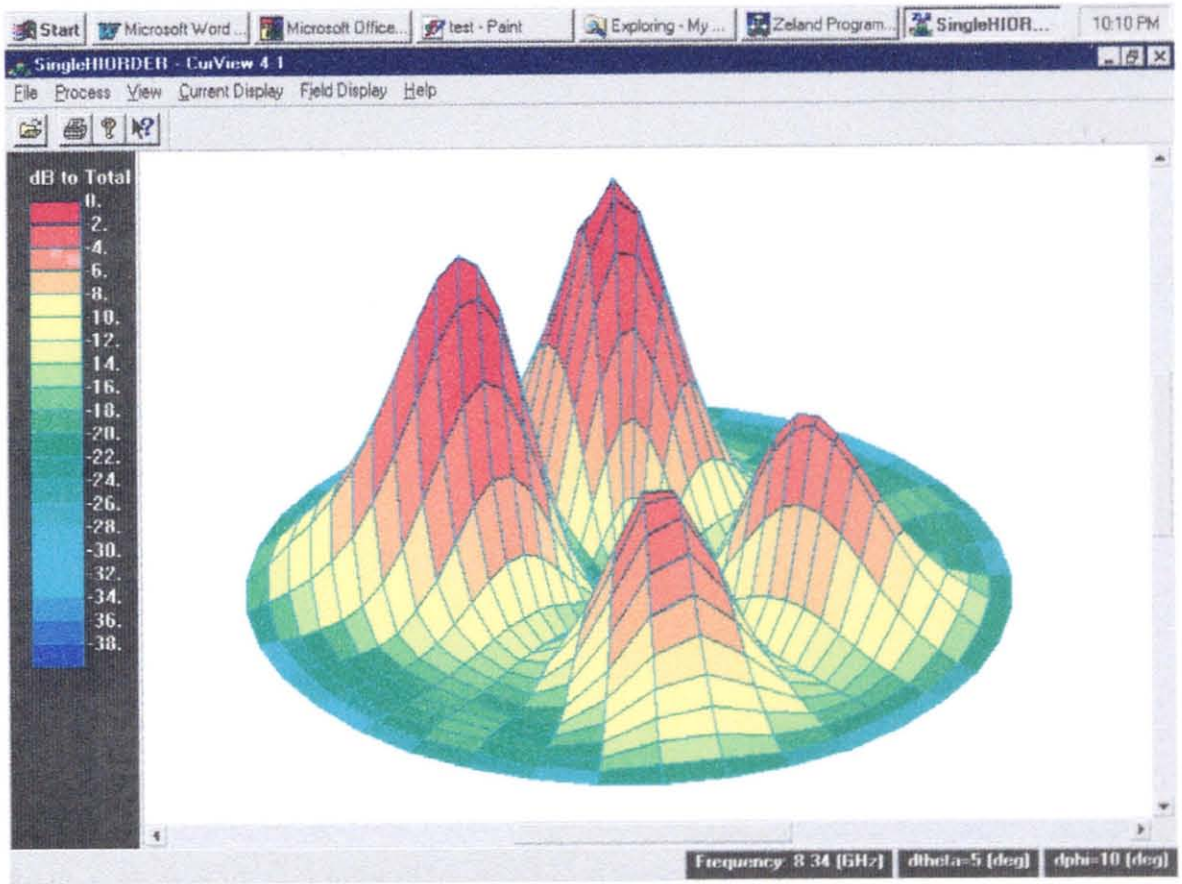

Figure 3.21 Radiation pattern corresponding to a 4th order of a microstrip patch antenna

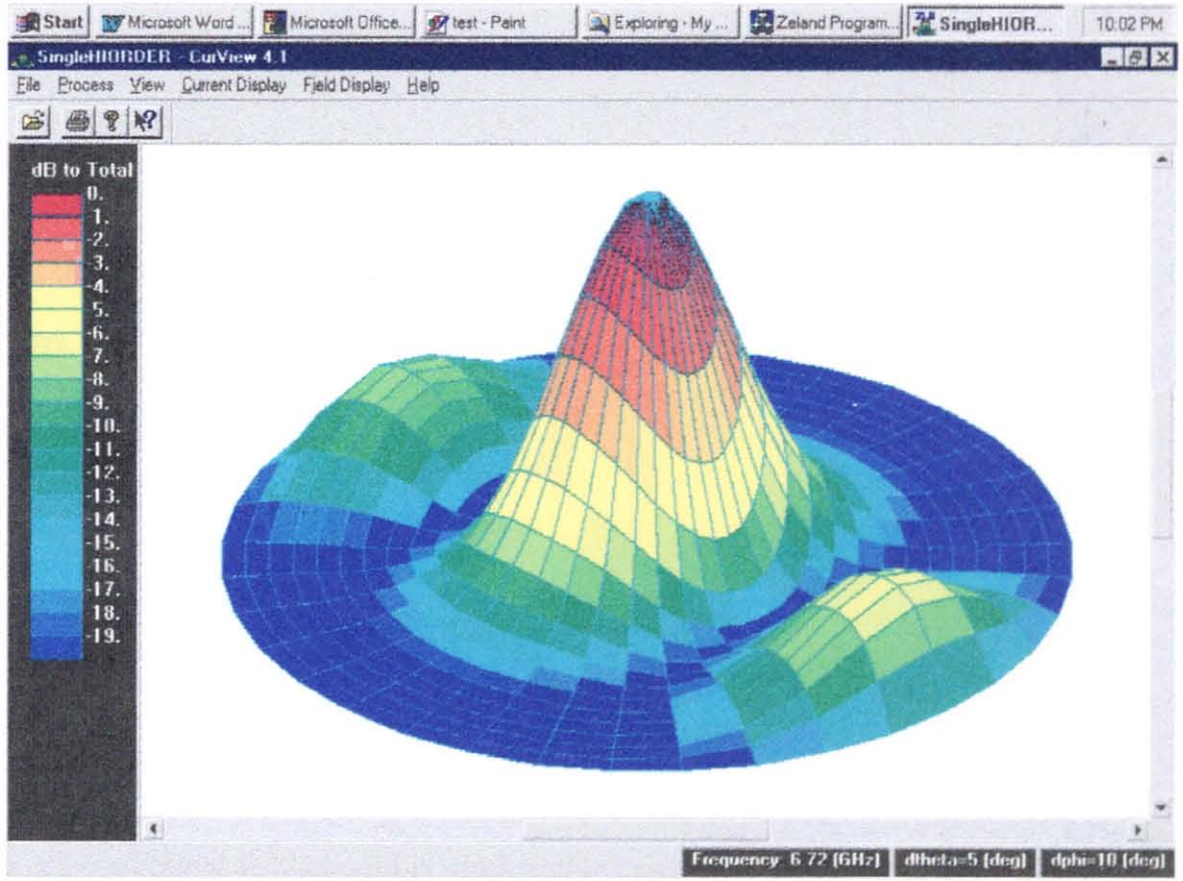

Figure 3.20 Radiation pattern corresponding to a 3rd order of a microstrip patch antenna

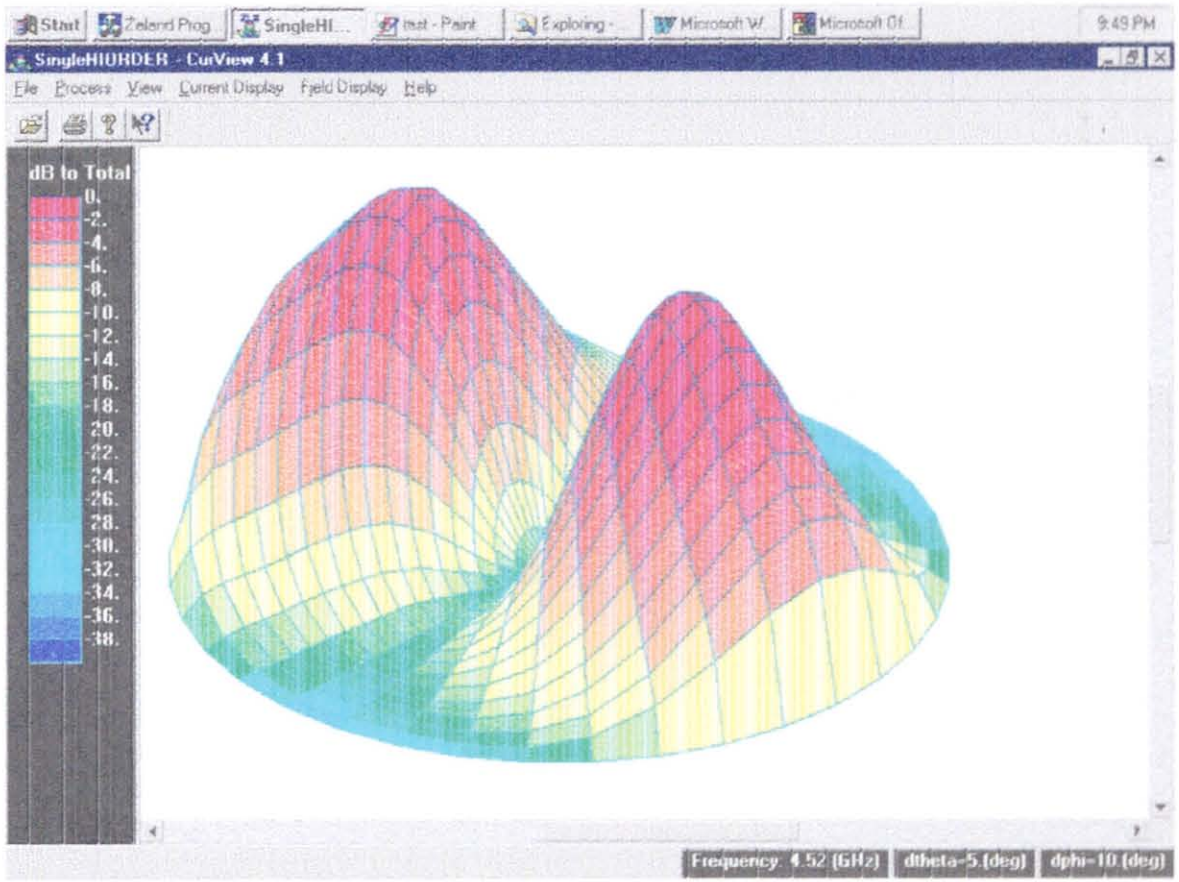

Figure 3.19 Radiation pattern corresponding to a 2nd order of a microstrip patch antenna

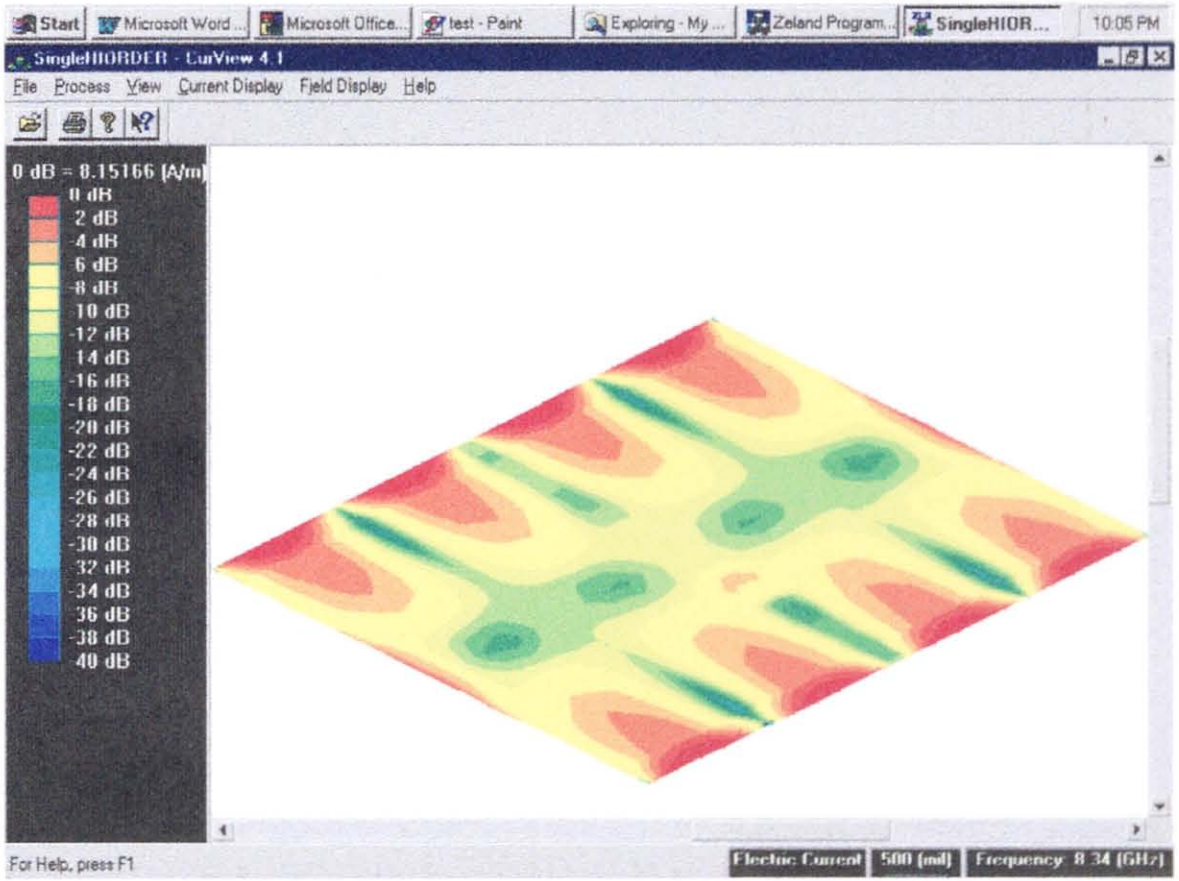

Figure 3.18 Current distribution of 4th order mode of a single patch microstrip antenna

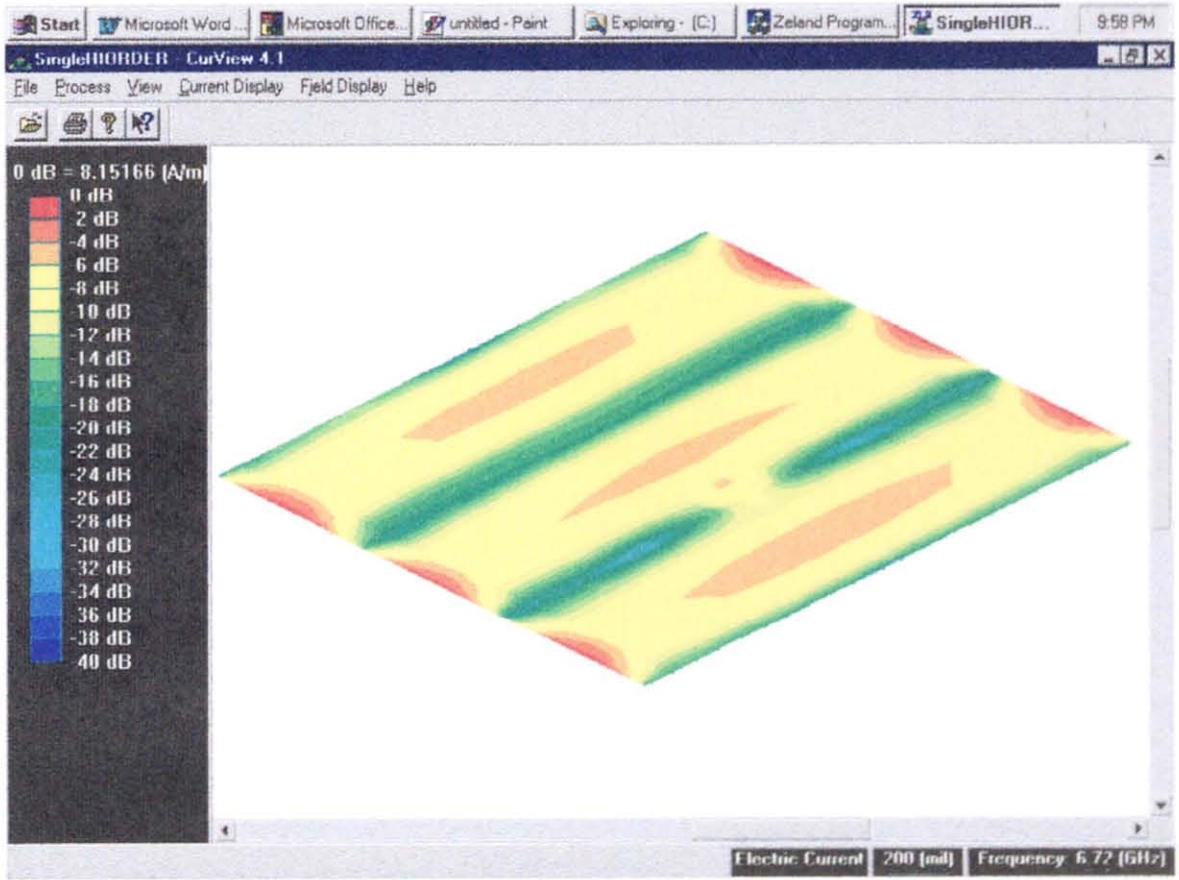

Figure 3.17 Current distribution of 3rd order mode of a single patch microstrip antenna

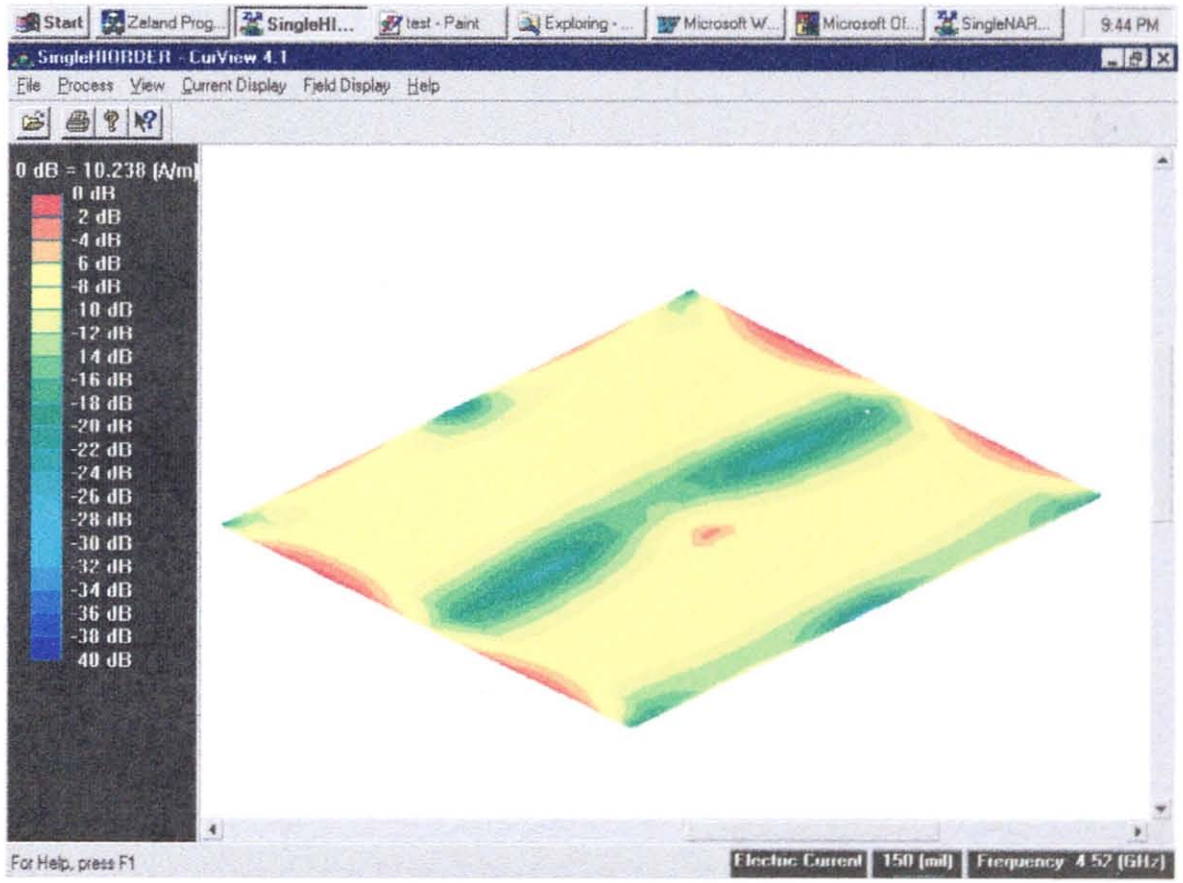

Figure 3.16 Current distribution of 2nd order mode of a single patch microstrip antenna

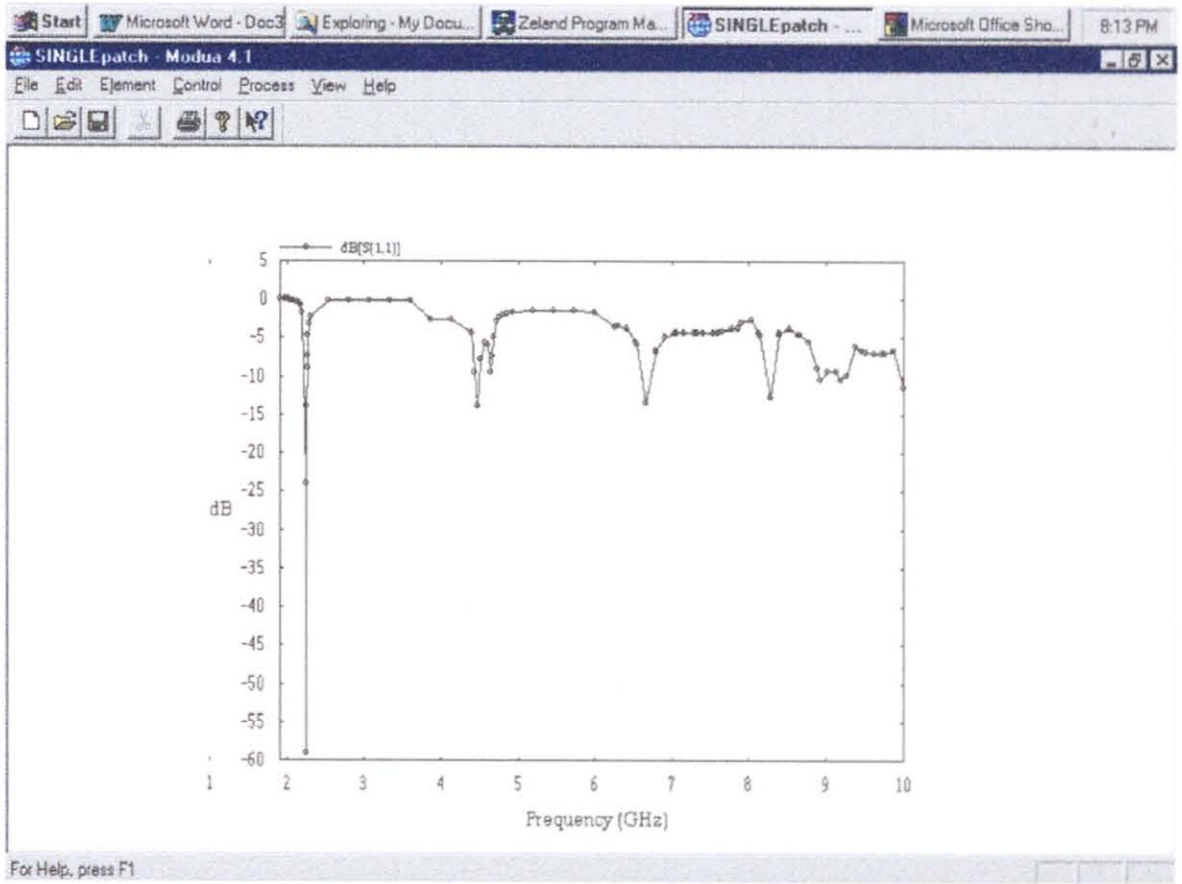

Figure 3.15 Wide band frequency response of the single patch probe feed antenna of Figure 3.7

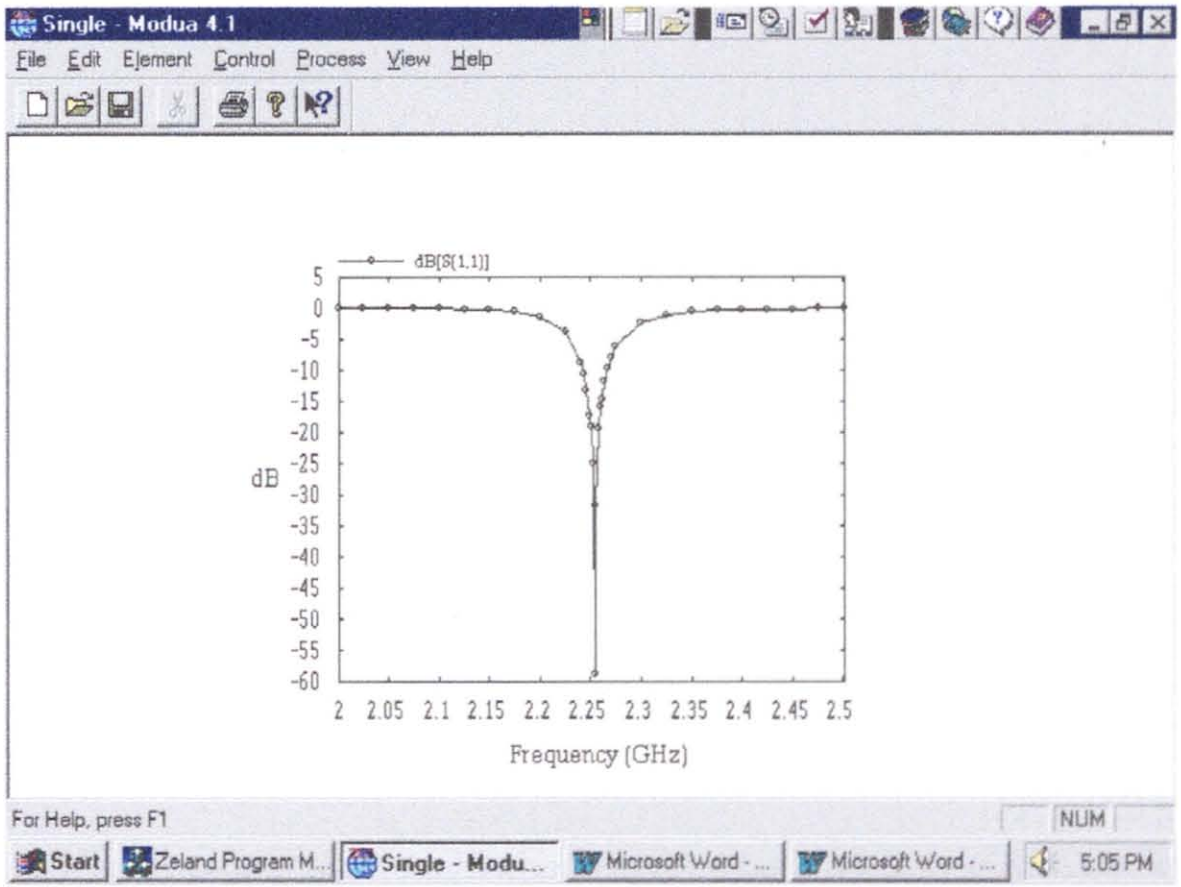

Figure 3.14 Return loss of single patch probe feed antenna of Figure 3.7

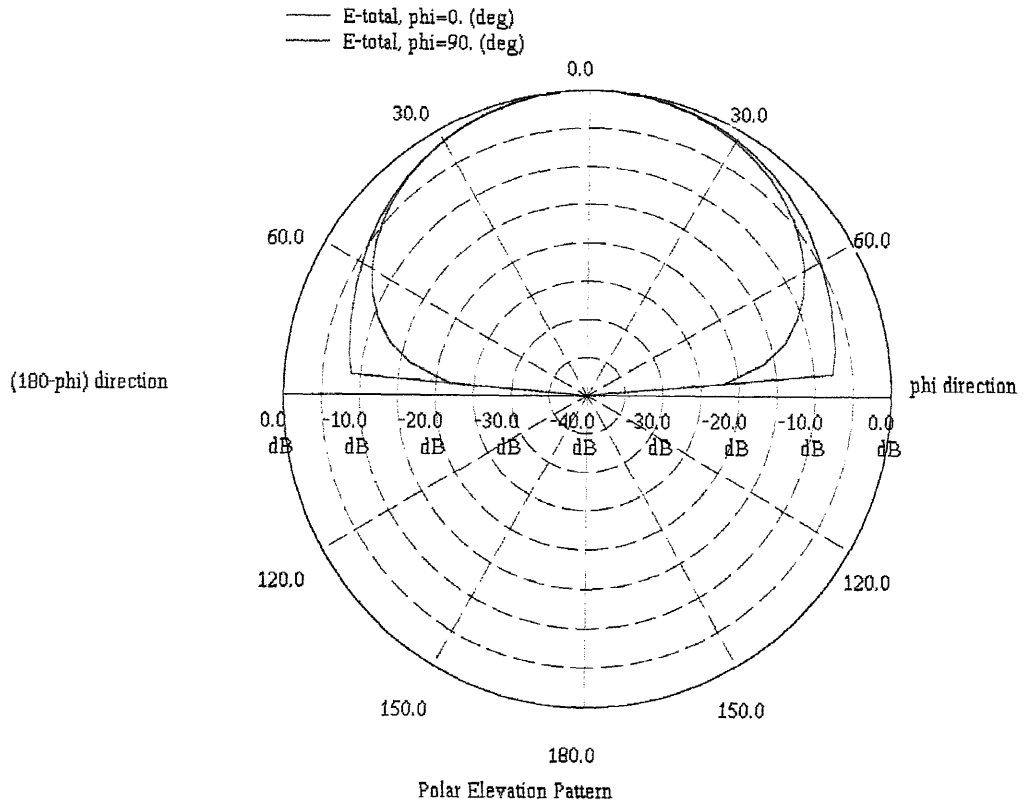

Figure 3.22 2-D polar radiation pattern of a single patch antenna for the fundamental mode at f = 2.254 Hz

CHAPTER 4

HYBRID (RAT-RACE) COUPLER

The hybrid coupler used in the zero-sum antenna can either be implemented using the microstrip or stripline configurations. For packaging purposes, the stripline implementation is more suitable to avoid any interference effects with its mount.

4.1 Stripline

The commonly used stripline technology is based on a strip conductor which is embedded into the dielectric slab and is sandwiched between top and bottom ground planes is shown in Figure 4.1 (a). Its characteristic impedance is given by [10]:

$$Z_0 = \frac{94.15}{\sqrt{\varepsilon_r}} \cdot \left(\frac{w}{d} \cdot K + \frac{C_f}{8.854\varepsilon_r} \right)^{-1}$$

where $$K = \frac{1}{1 - \frac{t}{d}}$$

$$C_f = \frac{8.854 \cdot \varepsilon_r}{\pi} \cdot \left[2K\ln(K+1) - (K-1) \cdot \ln\left(K^2 - 1\right) \right]$$

Unlike the microstrip line, stripline is a pure transverse electromagnetic mode structure. The realization of a stripline circuitry is less convenient than the counter part microstrip line because the dielectric substrate must be removed if one desires to include any additional discrete components and therefore the whole upper cover must also be completely removed. The tradeoff between these two types of lines are in their corresponding insertion losses. Due to quasi-TEM mode, microstrip line suffers excessive loss due to radiation loss in addition to dispersive material and waveguide losses at higher frequencies [13]. In the current application there is no need to place any lumped components in the hybrid ring therefore stripline hybrid ring is preferred over microstrip hybrid ring. However, attention has to be paid in maintaining the proper grounding due to top and bottom ground planes conductors.

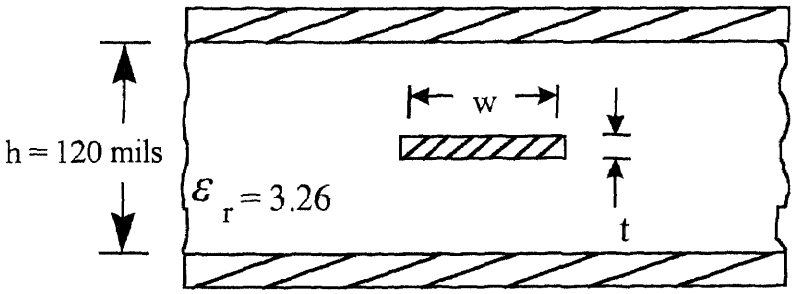

(a) Strip line

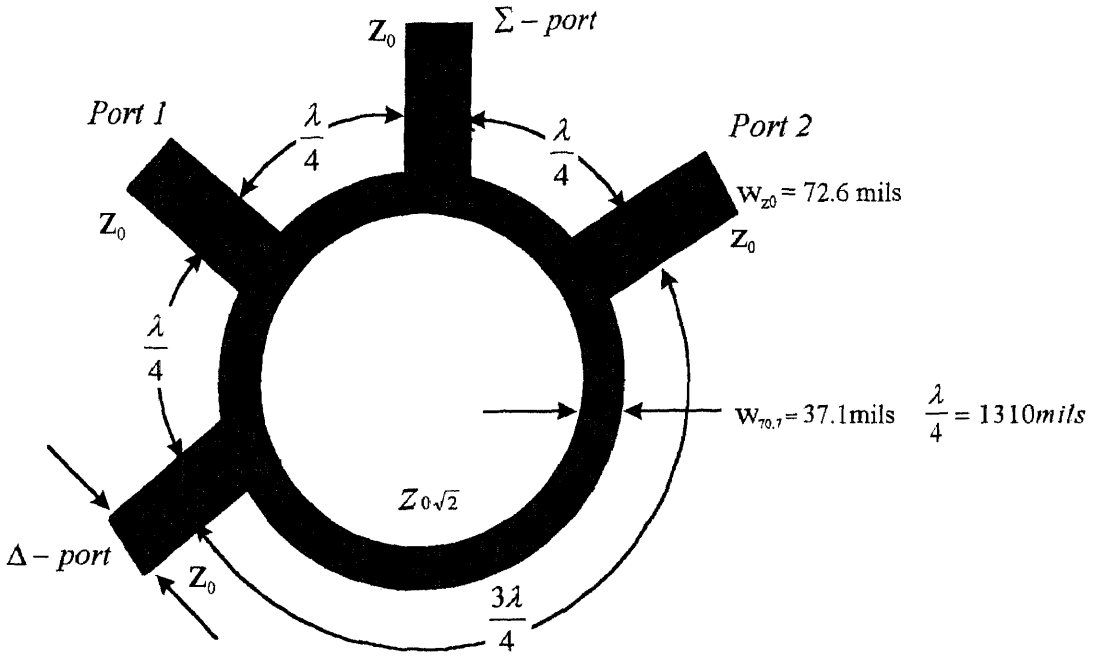

(b) Rat-race coupler

Figure 4.1 Stripline and stripline rat-race coupler.

4.2 Stripline Hybrid Ring Coupler

The stripline ring is a four port device that consists of a 1.5 wavelength perimeter length of a metal ring embedded at the center of a dielectric slab which is sandwiched between top and bottom conducting ground planes as shown in Figure 4.1 (b).

Input signals applied to port 1 and port 2 will be divided into two and travel in opposite directions. These signals will add up at the Σ-port and cancel out at the Δ-port if the lengths between the ports are chosen as in Figure 4.1 (b). By the same token, if an input signal is applied at the Σ-port, it will split the power equally to port 1 and port 2. Since there is no signal flowing into the Δ-port, it functions as an open circuit. The Σ-port, port 1, and port 2 all are terminated with 50 ohms. In order for the Σ-port to split the signal equally into both port 1 and port 2 and without encountering any reflections from them, the Σ-port must see at each junctions having 100 Ohms impedance connected parallel to it. A quarter-wave transformer with 70.7 Ohms characteristic impedance is needed to transfer 50 Ohms to 100 Ohms. The distance between port 1 and port 2 to the Σ-port is already a quarter wavelength The other requirement must be satisfied is that the characteristic impedance of the hybrid ring coupler should be 70.7 Ohms.

4.3 CAD Analysis of Stripline Hybrid Ring

Starting from the assumption that the hybrid ring (rat race) coupler has to have the total perimeter length of 3/2 λ, the final shape could either be a circular or oval (Figure 4.3) ensuring to elimination of the presence of possible sharp bends. As an initial choice, the oval shaped ring was used in the design as shown in Figure 4.3. However, an analysis in terms of the return losses at each port as shown in Figure 4.7 revealed that even though return loss at port 1 and port 2 exhibited minima at the desired frequency f = 2.254 GHz, the remaining ports yielded frequency shifts in their corresponding minima. This could be attributed to the cross coupling between various sections of the oval shaped coupler. To reduce these effects, a circular shaped coupler which will result in an increased coupling distance as shown in Figure 4.2 was analyzed. The results of Figure 4.5 achieved the desired goal that all ports have exhibited minimum return loss at desired frequency.

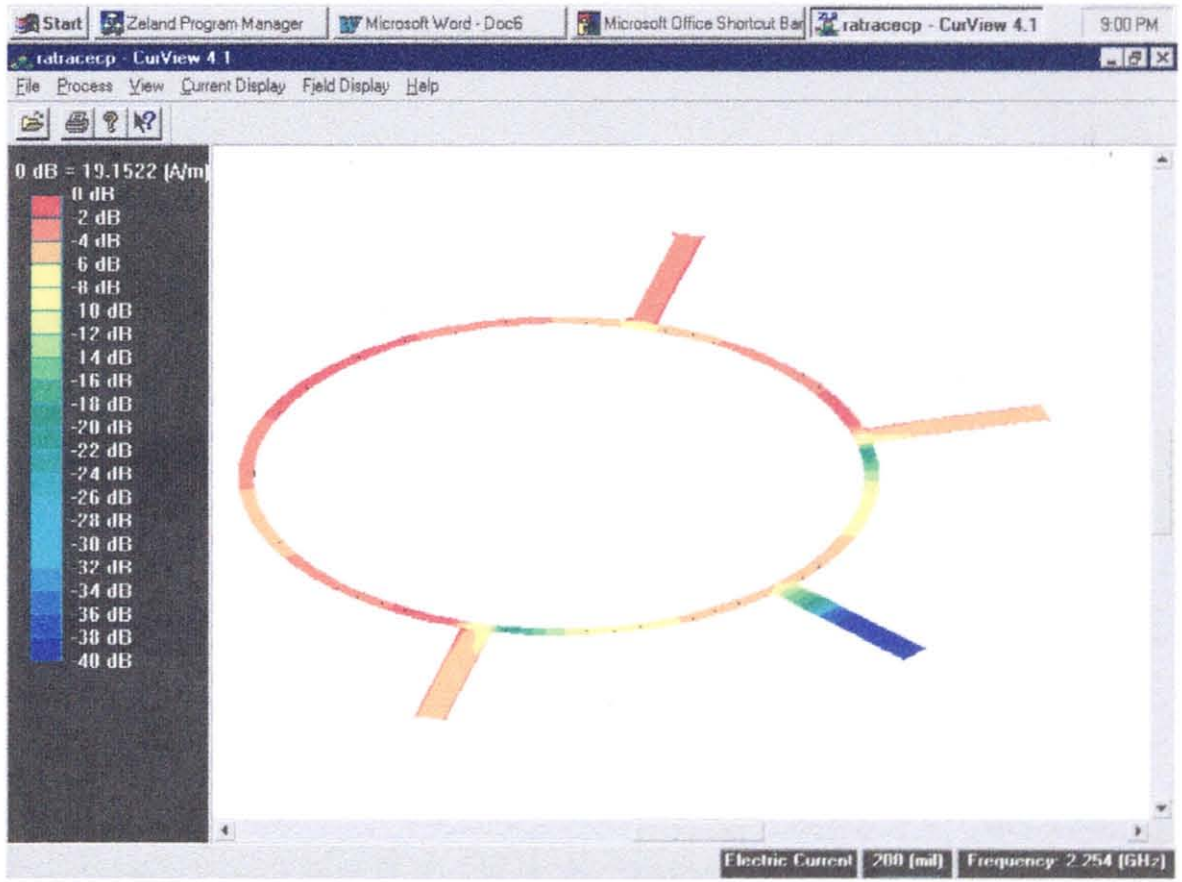

Figure 4.2 Current density distribution of the circular ring coupler of Figure 4.1

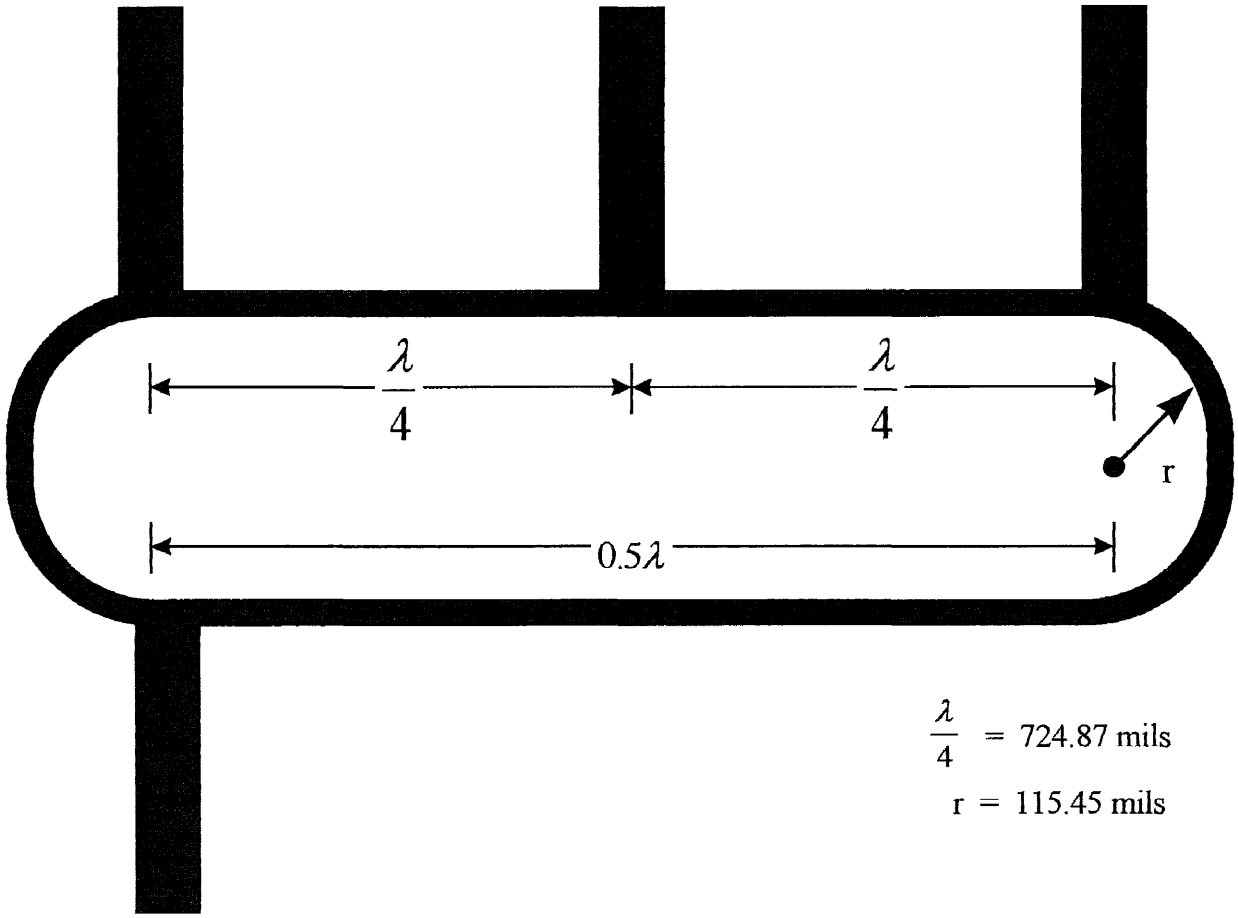

Figure 4.3 Oval shaped hybrid coupler

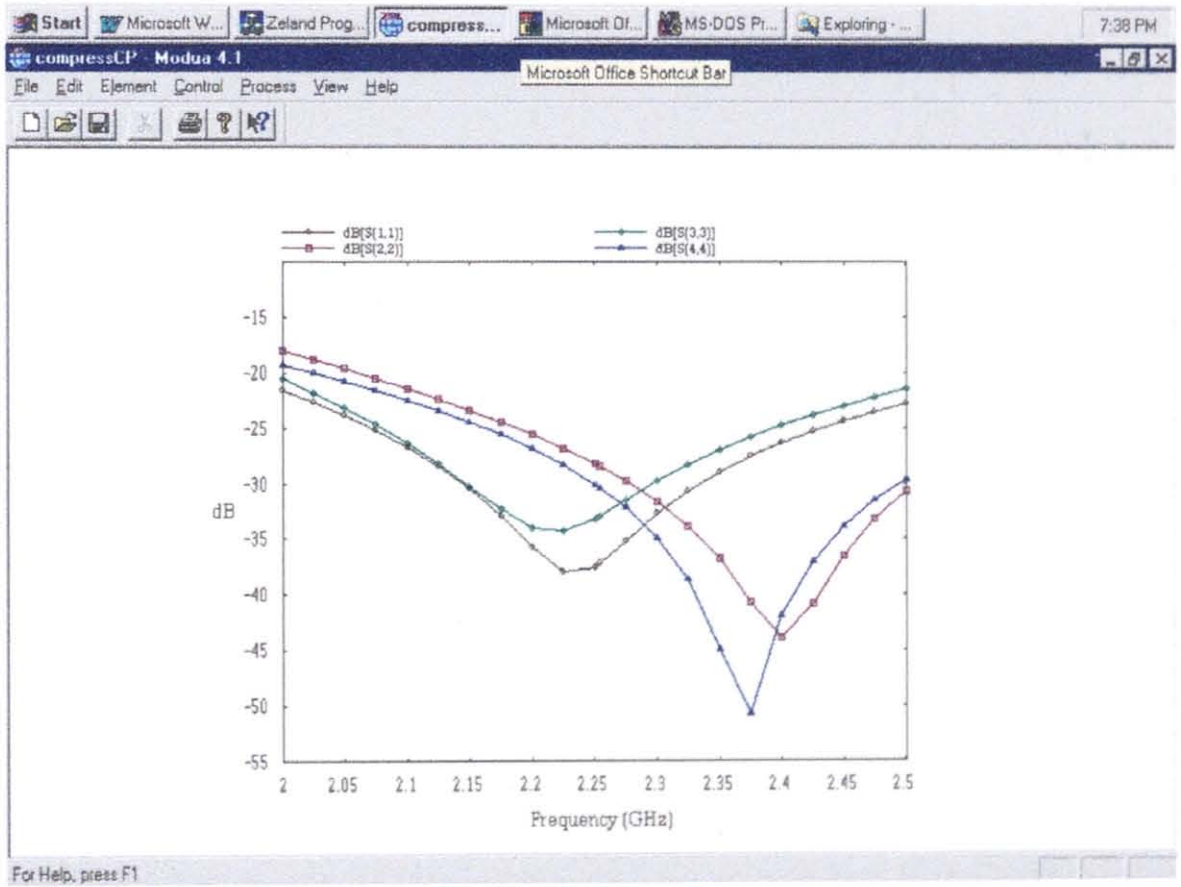

Figure 4.4 Return loss of the oval hybrid shaped coupler

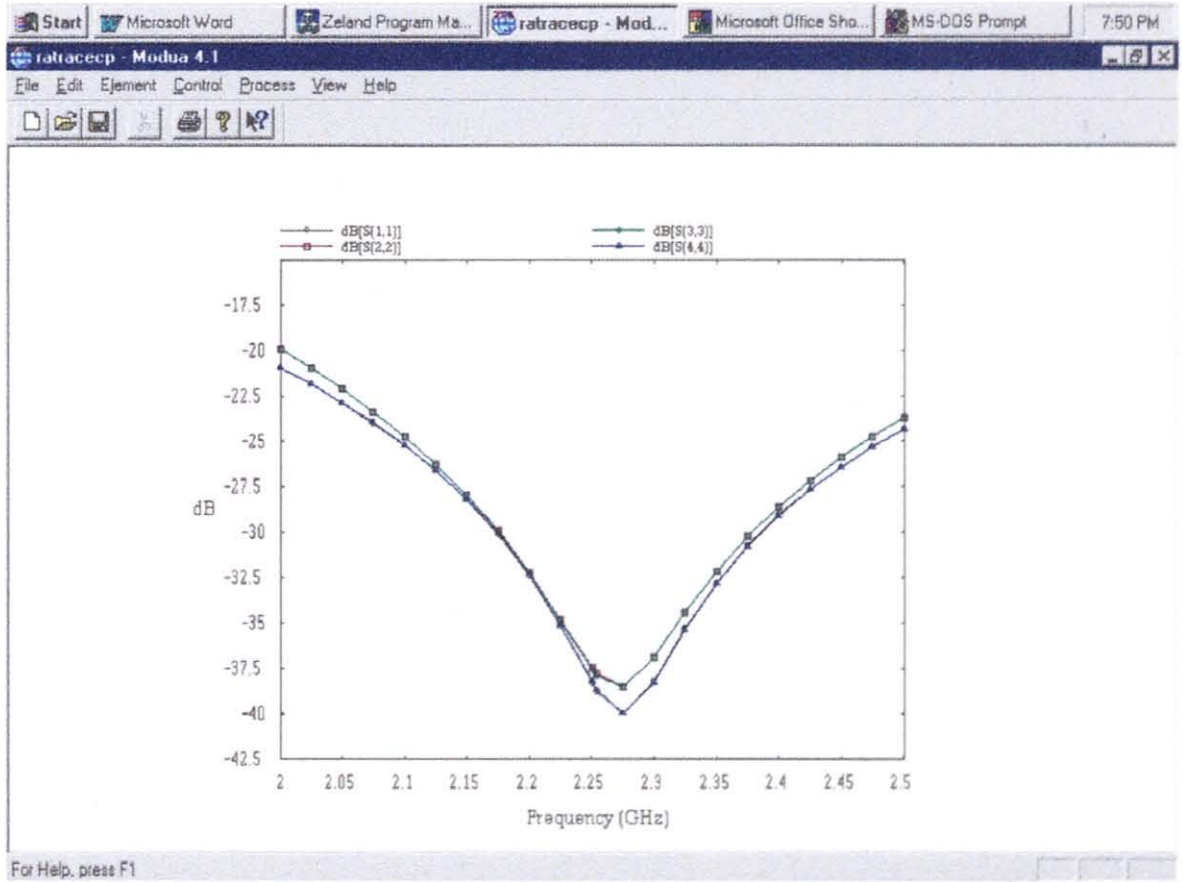

Figure 4.5 Return loss of the hybrid ring coupler of Figure 4.1

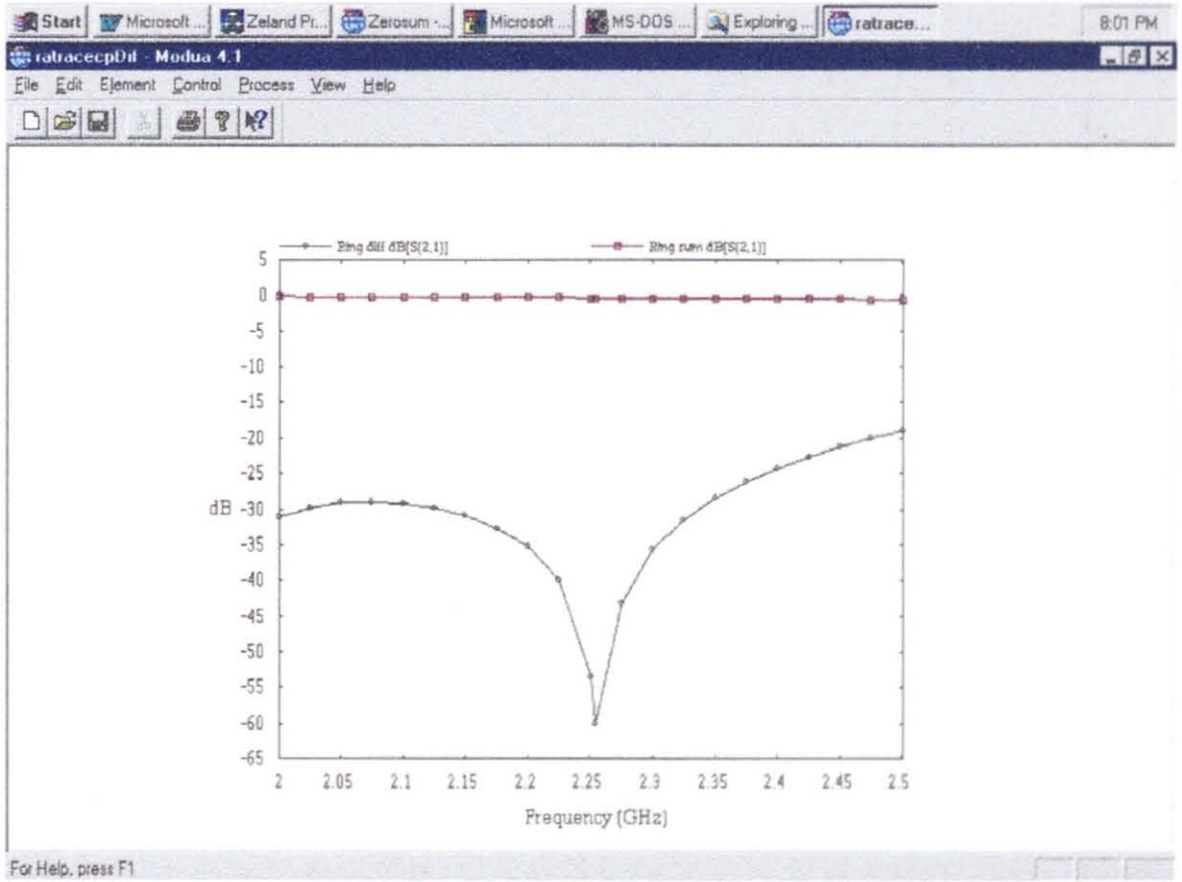

Figure 4.6 Sum and difference responses of the circular ring coupler of Figure 4.1

The performance characteristics of the couplers are not limited to the return loss only. Further analysis are carried out to check the ability of the coupler to add and subtract the two input signals. Figure 4.6 exhibits the frequency response at the Σ-port and the Δ-port due to signals of equal amplitude and phase applied at port 1 and port 2. The Δ-port yielded -60 dB, implying very good cancellation, while the Σ-port yielded summation around 0.5 dB. Similar results with significantly decreased performance were observed for the oval shaped coupler. The comparison between these two shaped couplers are shown in Figure 4.7 and 4.8 yielding 20 dB and 0.1 dB difference at the Δ-port and the $\sum$ port, respectively.

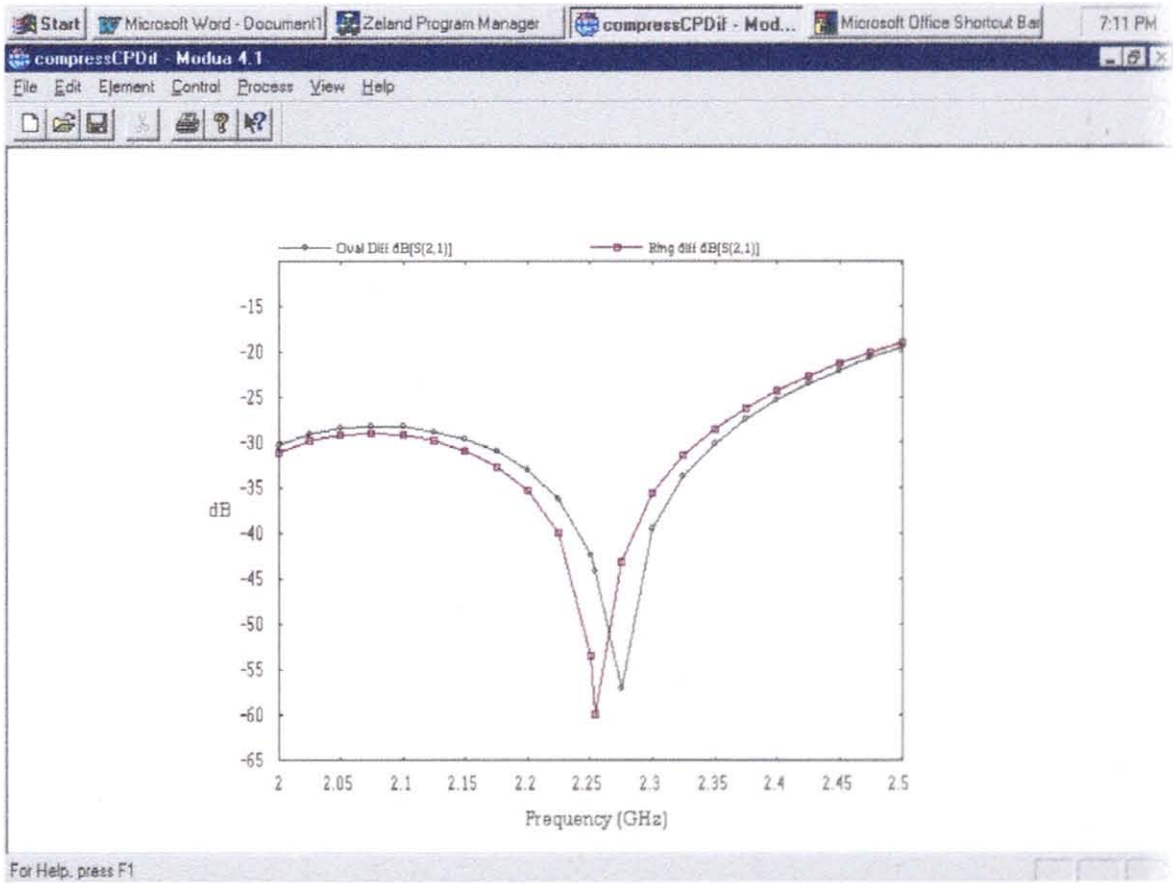

Figure 4.7 Comparison between difference responses of circular and oval shaped ring

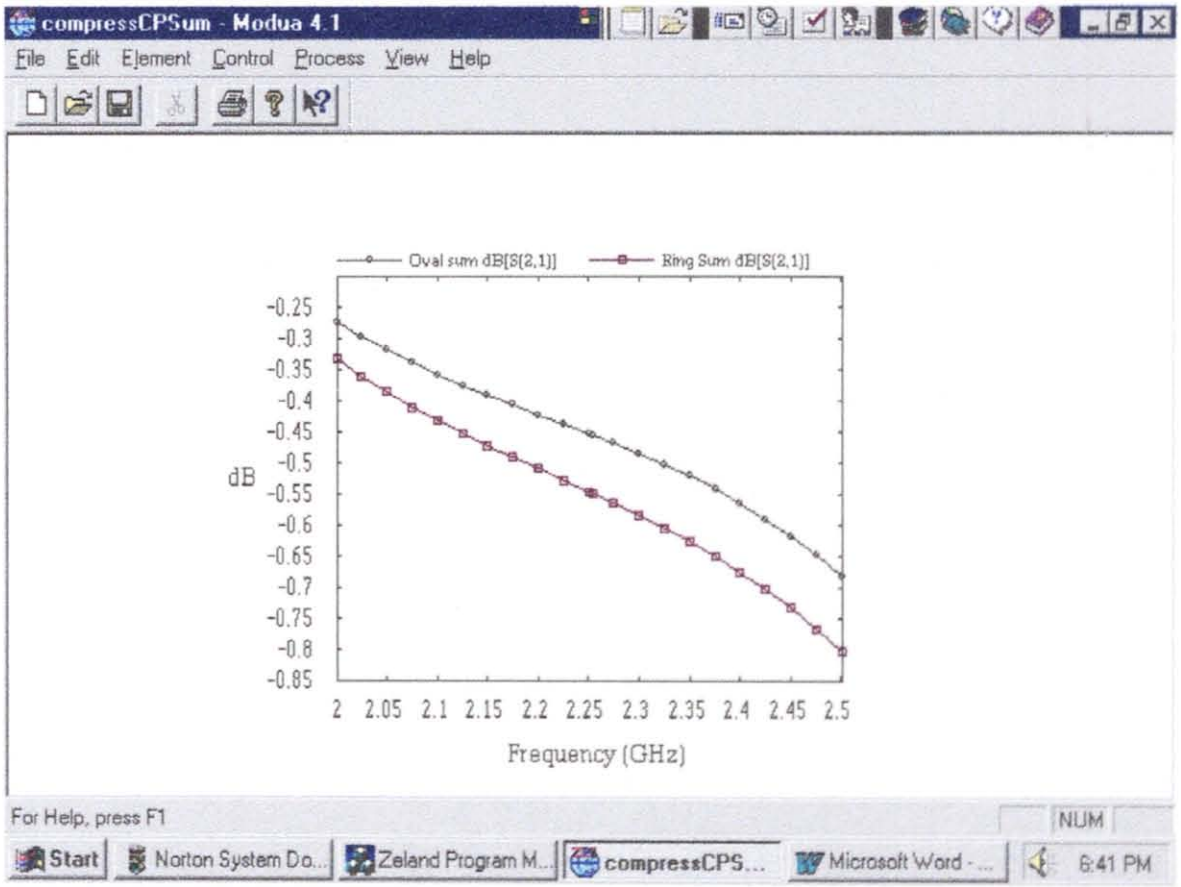

Figure 4.8 Comparison between summation responses of circular and oval shaped hybrid coupler of Figure 4.1 and 4.3, respectively

CHAPTER 5
EXPERIMENTAL RESULTS

The zero-sum antenna analyzed in previous chapters has been constructed using MC5 material provided by Glasteel Industrial laminates, Collierville, TN. The technical specification of this substrate material is attached in Appendix A. The microstrip patch antennas were etched on a material with ε_r=3.26 and thickness t=60 mils.

5.1 Antenna Elements

The two element array which forms the zero-sum antenna can be achieved using E-plane or H-plane coupling arrangements as shown in Figure 5.1. For inter-element spacing of $\lambda/2$ between the antennas as shown in Figure 5.1, the simulation results using IE3D are shown in Figure 5.2 reveal that H-plane coupling yields 5 dB better isolation between two antenna elements than the E-plane coupling. In many applications, the physical requirements may also dictate that the H-plane arrangement be used because of system and packaging requirements. From now on, H-plane coupling will be used with $\lambda_0/2$ spacing between the feed points but not between the edges as in Figure 5.1. Figure 5.3 corresponds to isolation between two patch elements placed $\lambda_0/2$ apart in free space obtained from IE3D simulation.

Corresponding experimental results shown in Figure 5.4 reveals that -16.0 dB isolation at f=2.254 GHz is almost in perfect agreement with the isolation of -16.5 dB from Figure 5.3.

Individual tuning has been applied on each element to achieve resonance at f=2.254 GHz. As seen in Figure 5.5, the return loss in the vicinity of -25 dB was measured for each antenna element.

5.2 The Hybrid (Rat-Race) Ring Coupler

The stripline hybrid ring coupler was fabricated on a combination of two layers GIL 5 boards resulting in a height of h=120 mils. The experimental performance of a coupler

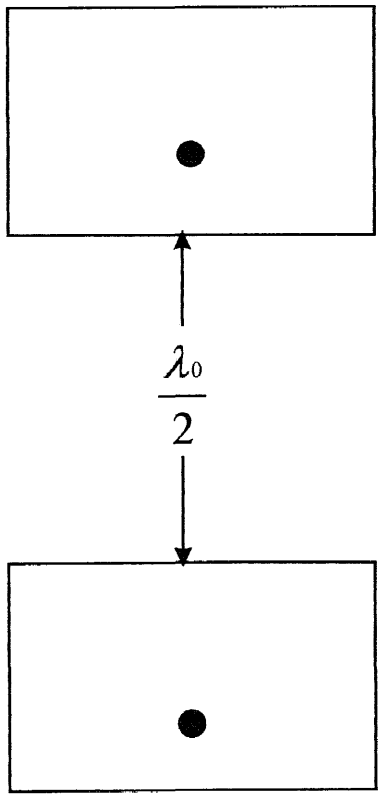

(b) E-plane mutual coupling

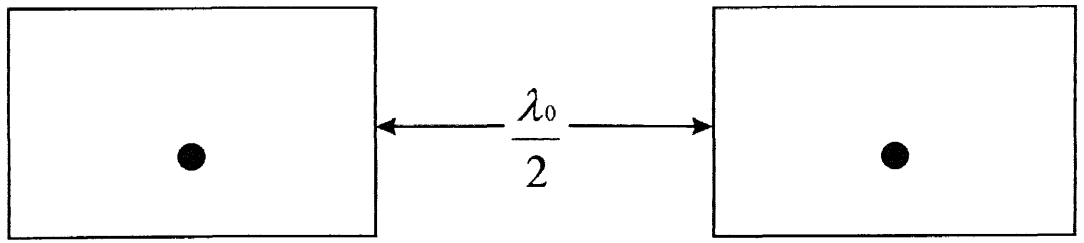

(b) H-plane mutual coupling

$$\frac{\lambda_0}{4} = 1310 \text{ mils}$$

Figure 5.1 E and H planes mutual coupling arrangements.
Elements parameters are chosen as in Figure 3.7.

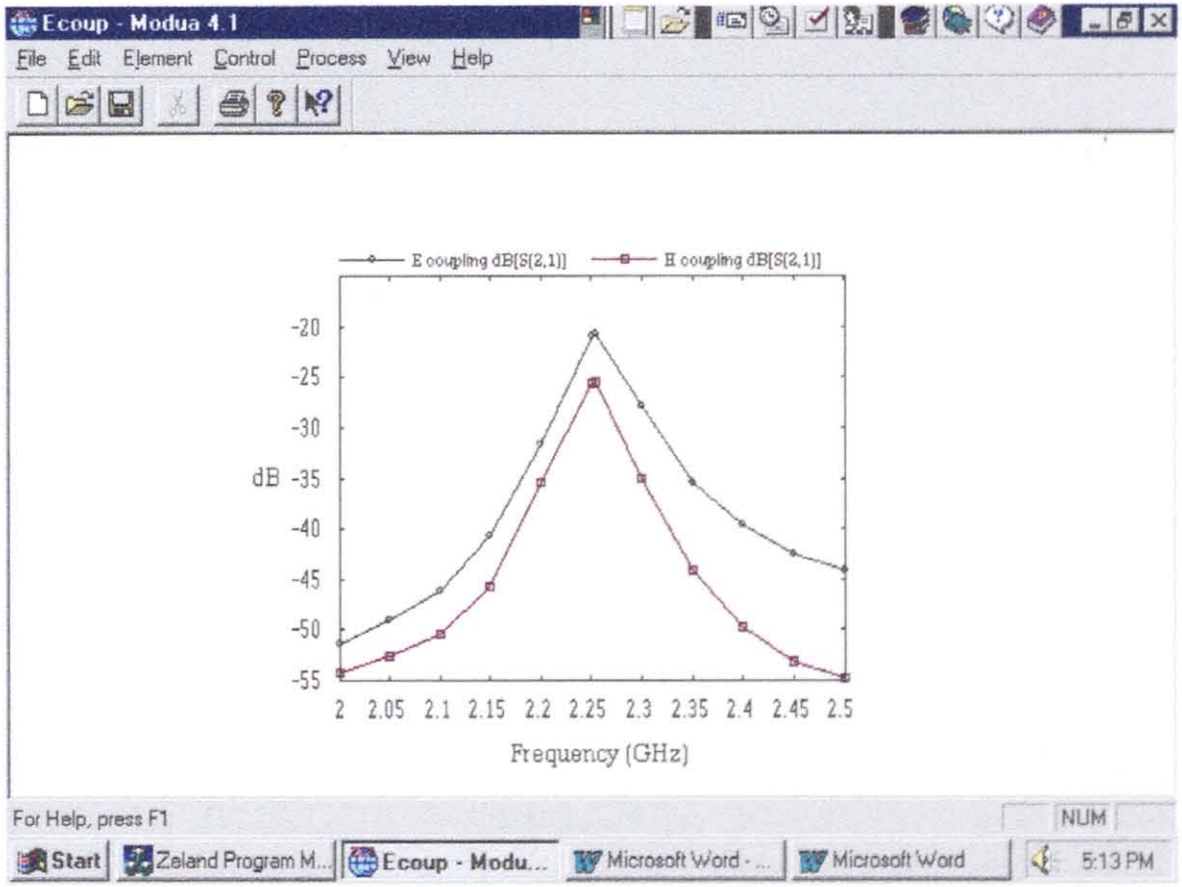

Figure 5.2 Isolation response for E and H planes coupling arrangement of Figure 5.1

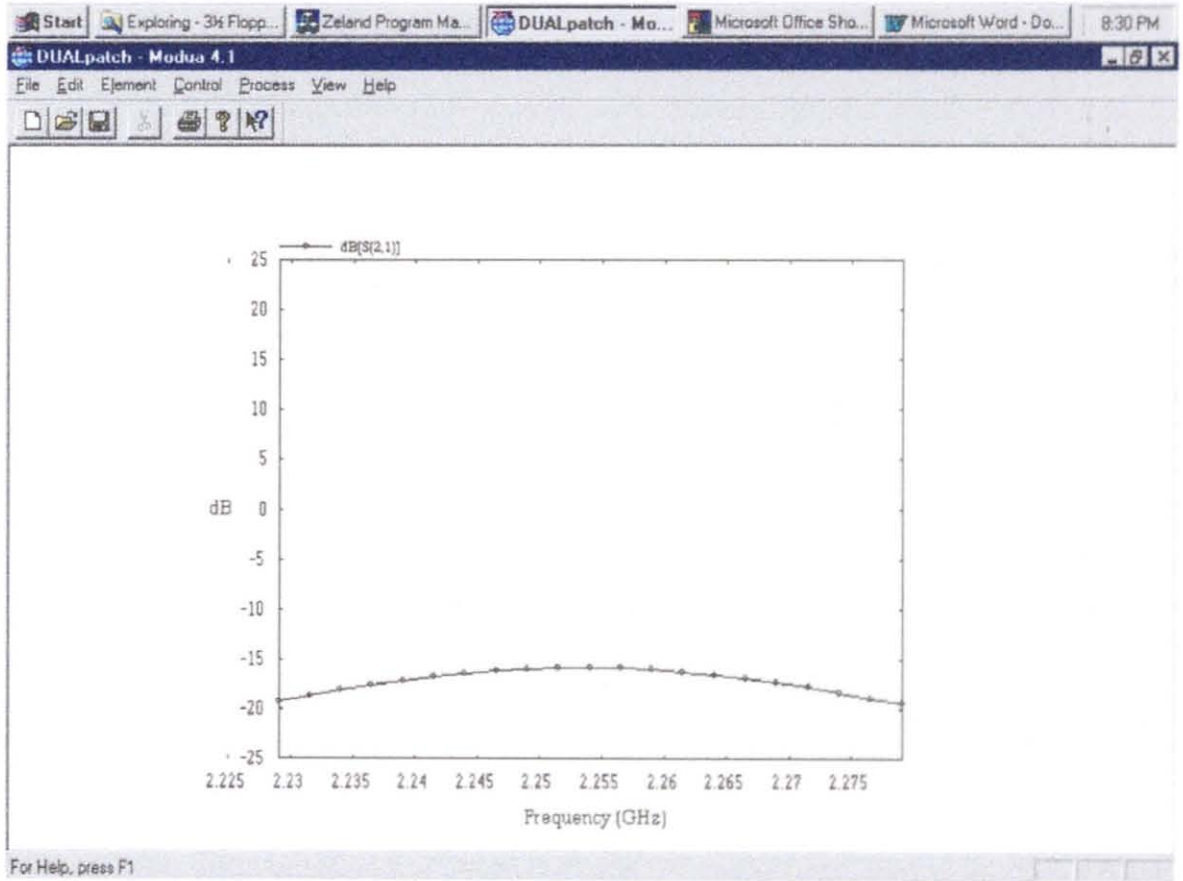

Figure 5.3 Isolation between two elements spaced λo/2 for H-plane mutual coupling based on simulation using ie3d

responses when port 1 and port 2 are excited by a signal of equal amplitude and phase are shown in Figure 5.6. Experimental results exhibit less than 3 dB insertion loss in Σ-port and the measured signal at the difference port turned out to be -21.9 dB. Corresponding matching characteristics at Σ-port and Δ-port yielded VSWR less than 2 at each port, respectively as seen in Figure 5.7.

5.3 Zero-Sum Antenna

Since, the antenna is a reciprocal device, its characteristics can be classified using it either in a receiving or transmitting mode. The graphical sketches of the current density and its vector representation for a zero-sum antenna excited at the Σ-port are given in Figure 5.8 and Figure 5.9, respectively. Similar sketches for the Δ-port are given in Figure 5.10 and 5.11, respectively. In each case, the unexcited other port is terminated by a matched load. The observed results of Figure 5.8 to 5.11 are in agreement with the predicted results by the cavity model due to the fundamental mode excitation.

In a zero-sum antenna, a good measure of performance is the corresponding return loss at the Σ-port and the Δ-port. The simulation results in Figure 5.12 exhibited that there is approximately 10 dB higher loss at the Σ-port compared to the Δ-port. This can be attributed to sharper interference patterns at the Σ-port compared to the Δ-port. Interestingly, a very similar pattern has been observed during the experimental measurements, resulting in almost 10 dB difference, between these two ports. The shift in the resonance can be attributed due to design errors in the coupler, since antenna elements have been checked experimentally in terms of their resonance frequencies

Far-field patterns are of utmost importance in the operation of a zero-sum antenna. Simulated results of the Figure 5.13 showed that a difference of 40 dB exists between the sum and zero patterns in the forward direction. Experimental results confirmed that functionality of the zero-sum antenna yielding corresponding difference of better than 20 dB which is adequate for the intended application. It is worthwhile to add that the resulting beamwidths obtained by measurements are in good agreement with the ones observed during simulation.

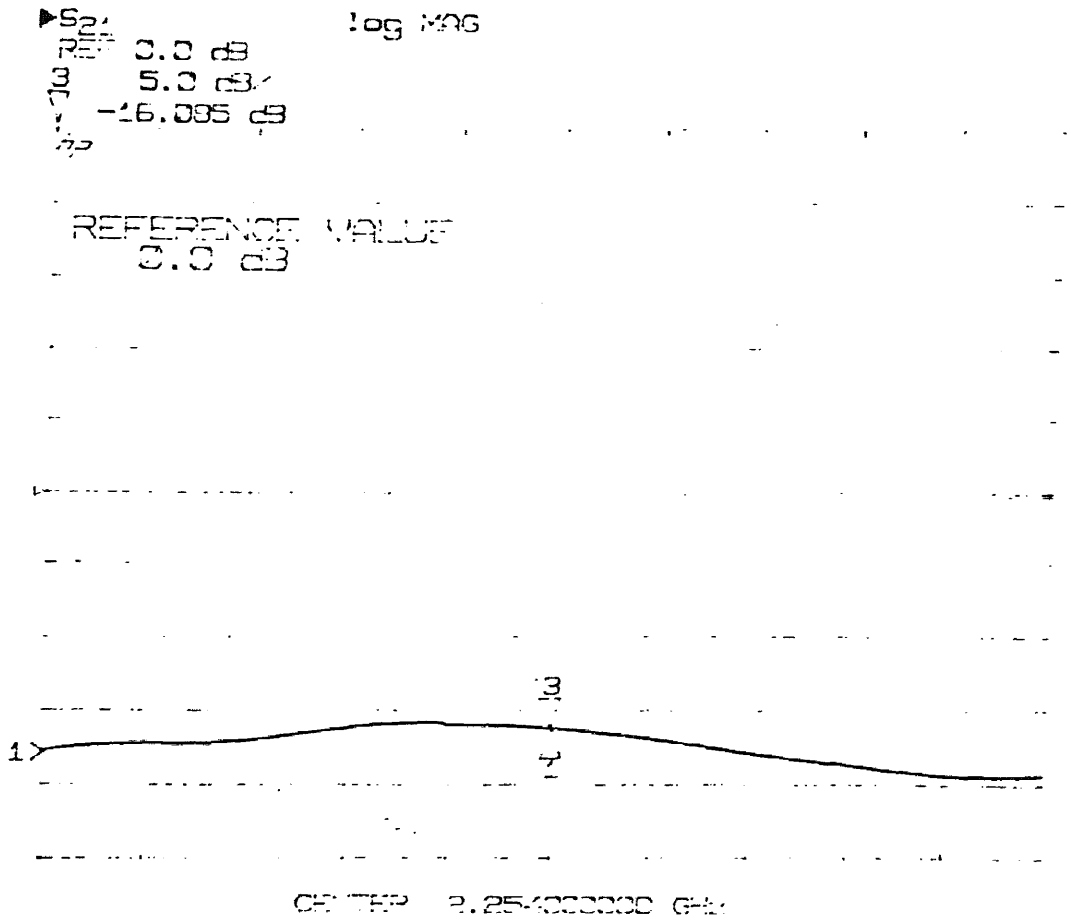

Figure 5.4 Experimental results of H-plane isolation between two elements spaced λo/2 apart

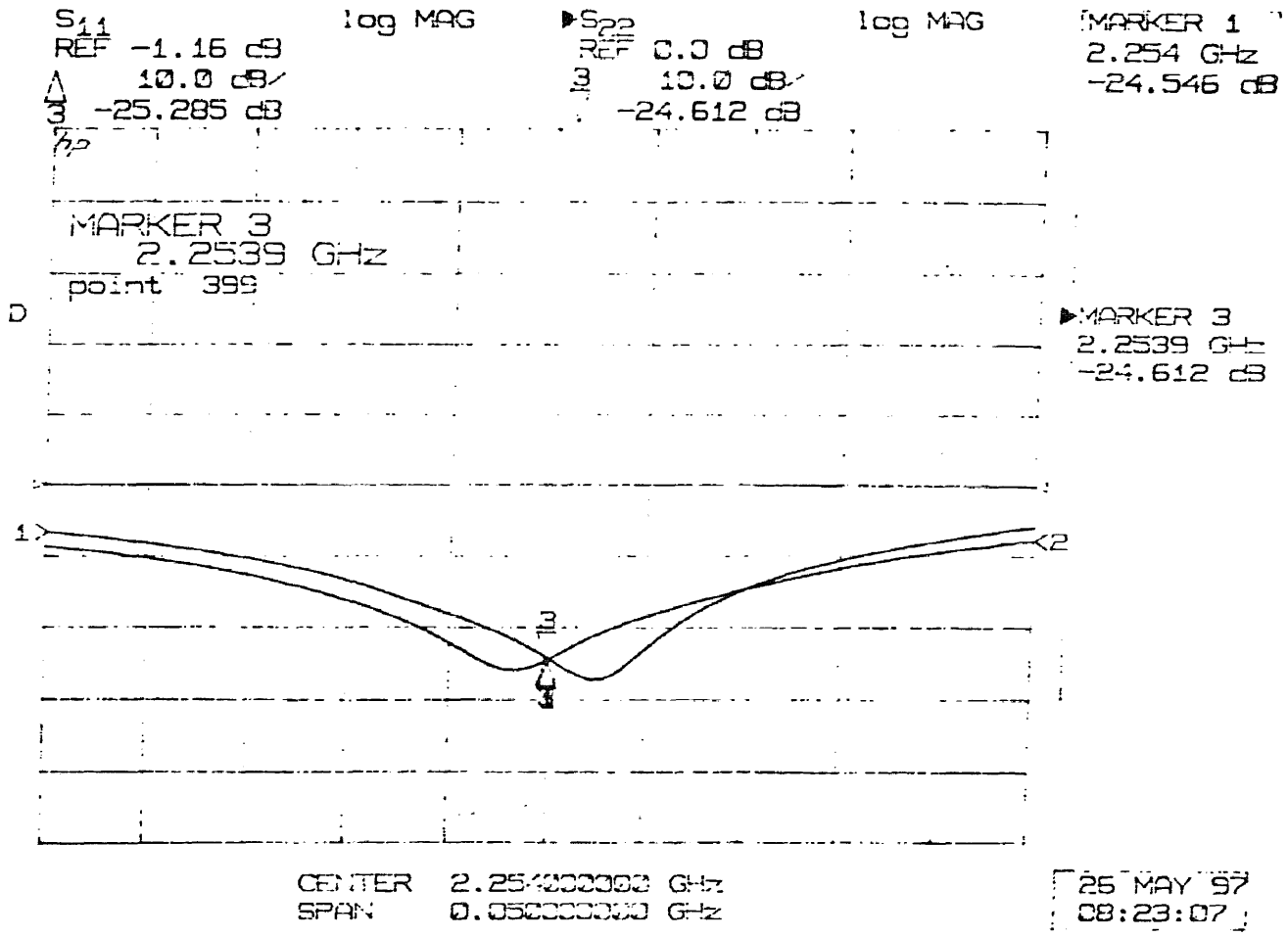

Figure 5.5 Experimental return loss for elements 1 and 2 in a zero-sum antenna versus frequency

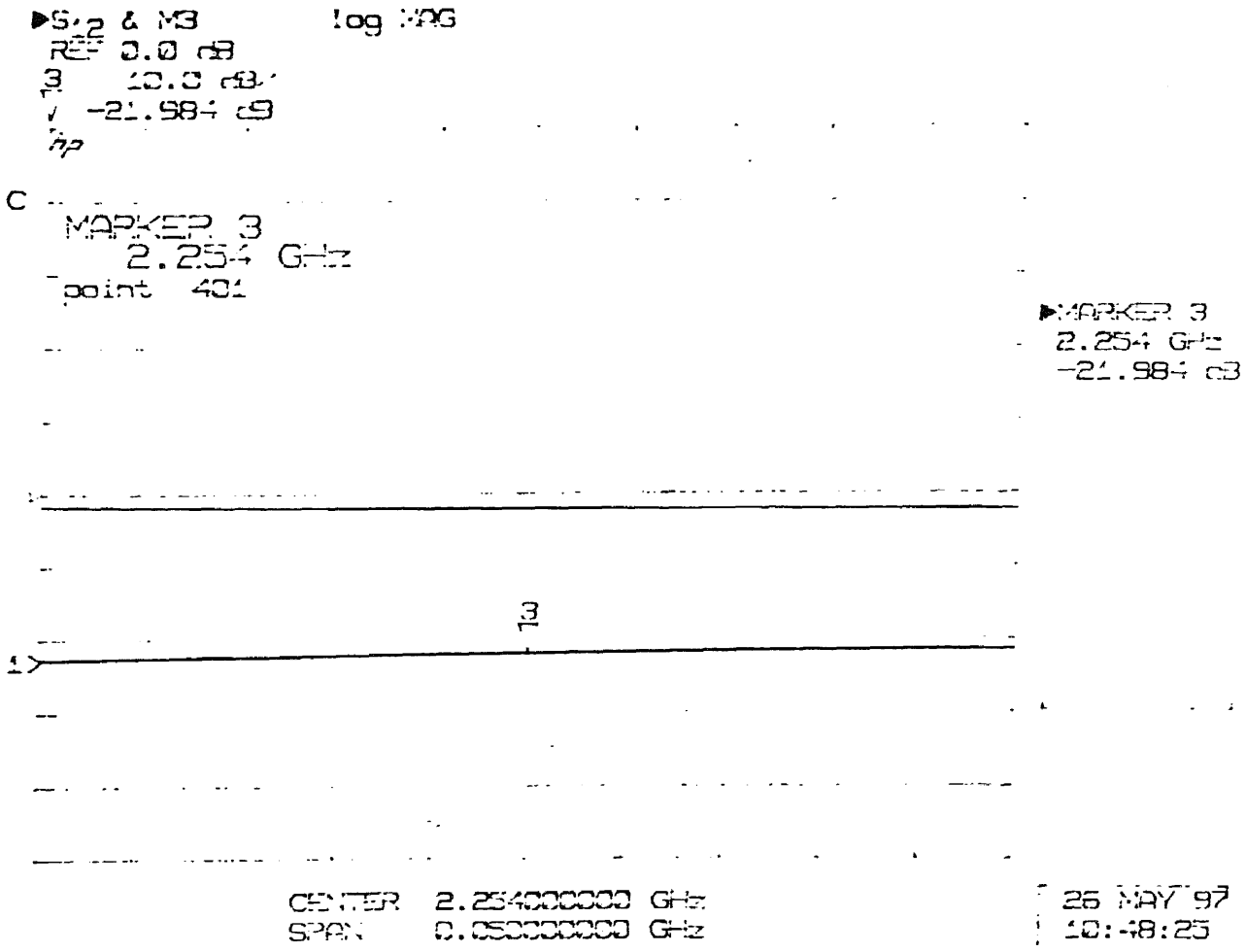

Figure 5.6 Experimental sum and difference response of a circular ring coupler of Figure 4.1

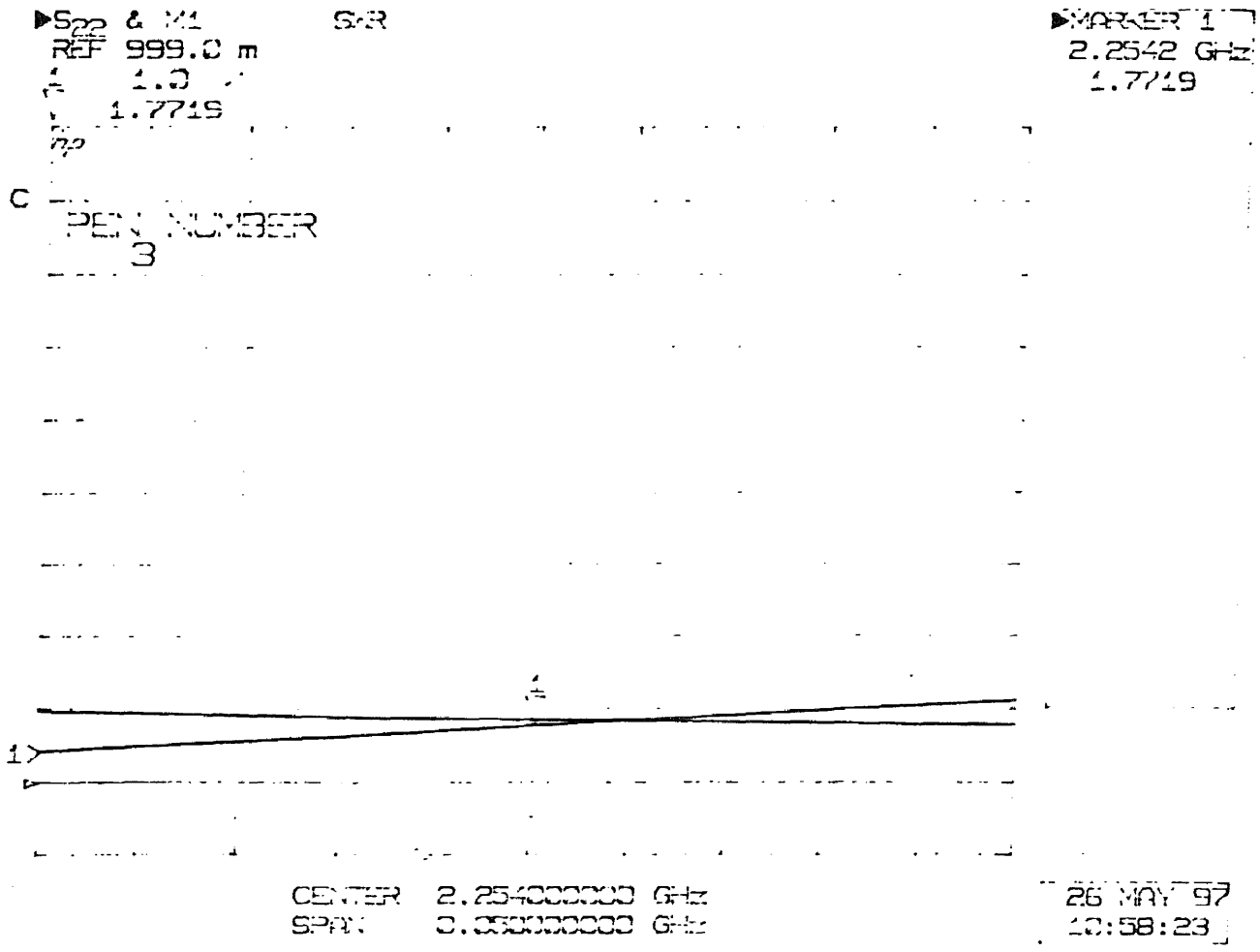

Figure 5.7 SWR at Σ - and Δ - ports of the manufactured coupler

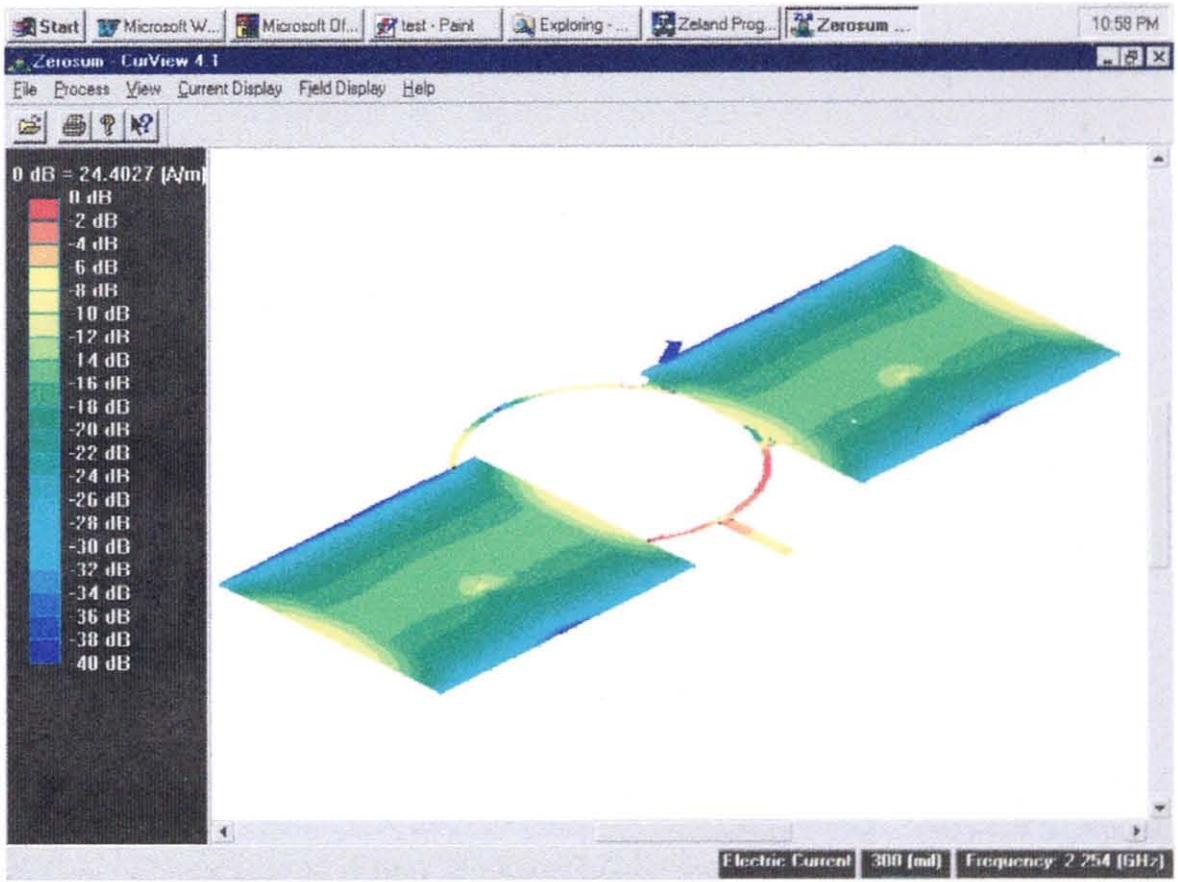

Figure 5.8 Current density distribution of a zero-sum antenna excited at Δ- ports

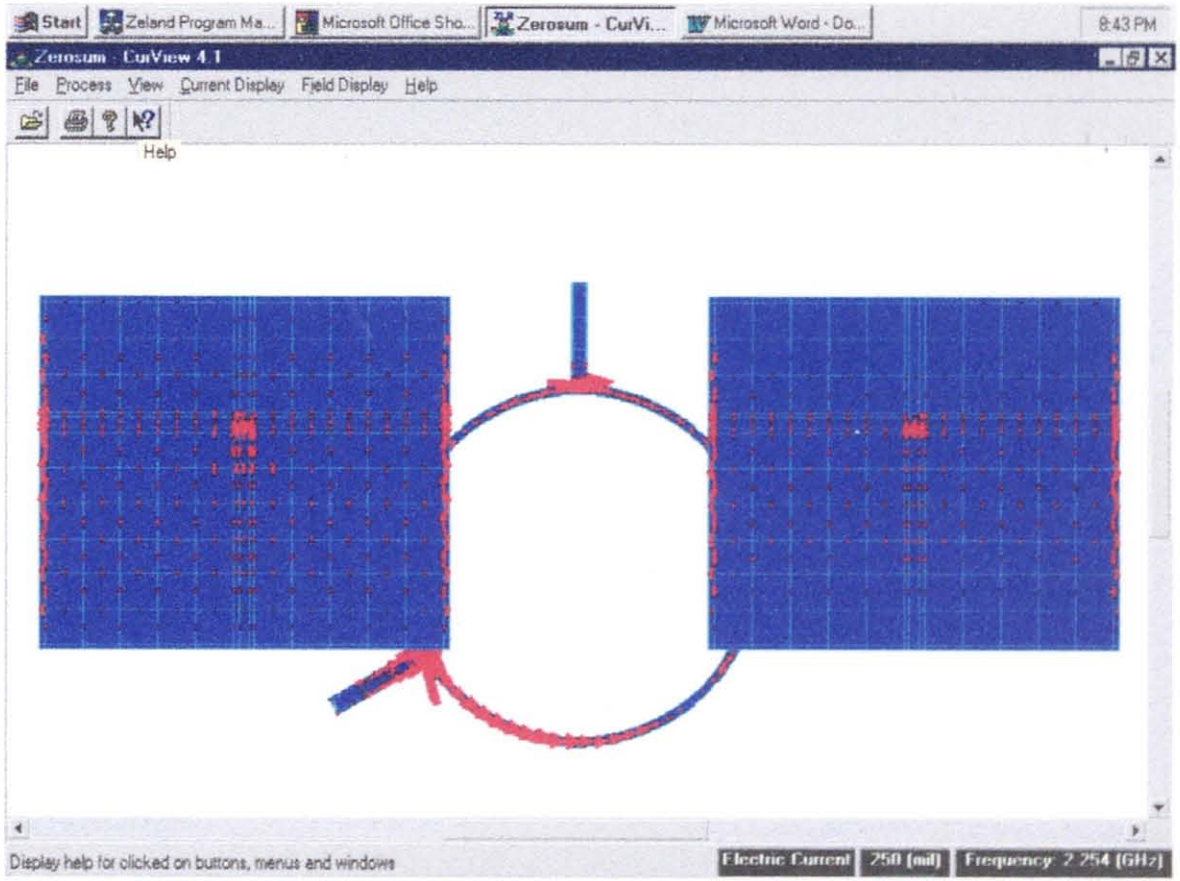

Figure 5.9 Current vector distribution of a zero-sum antenna excited at Δ- ports

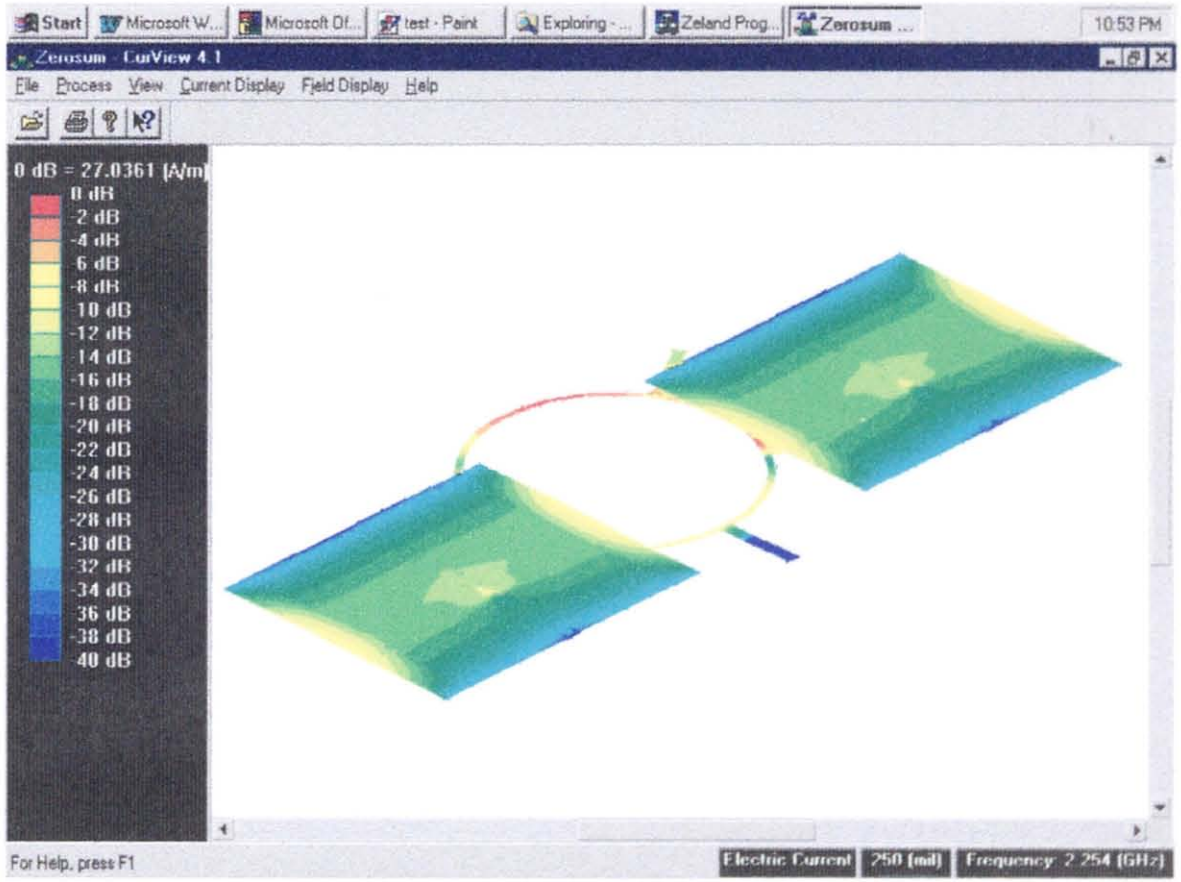

Figure 5.10 Current density distribution of a zero-sum antenna excited at Σ- ports

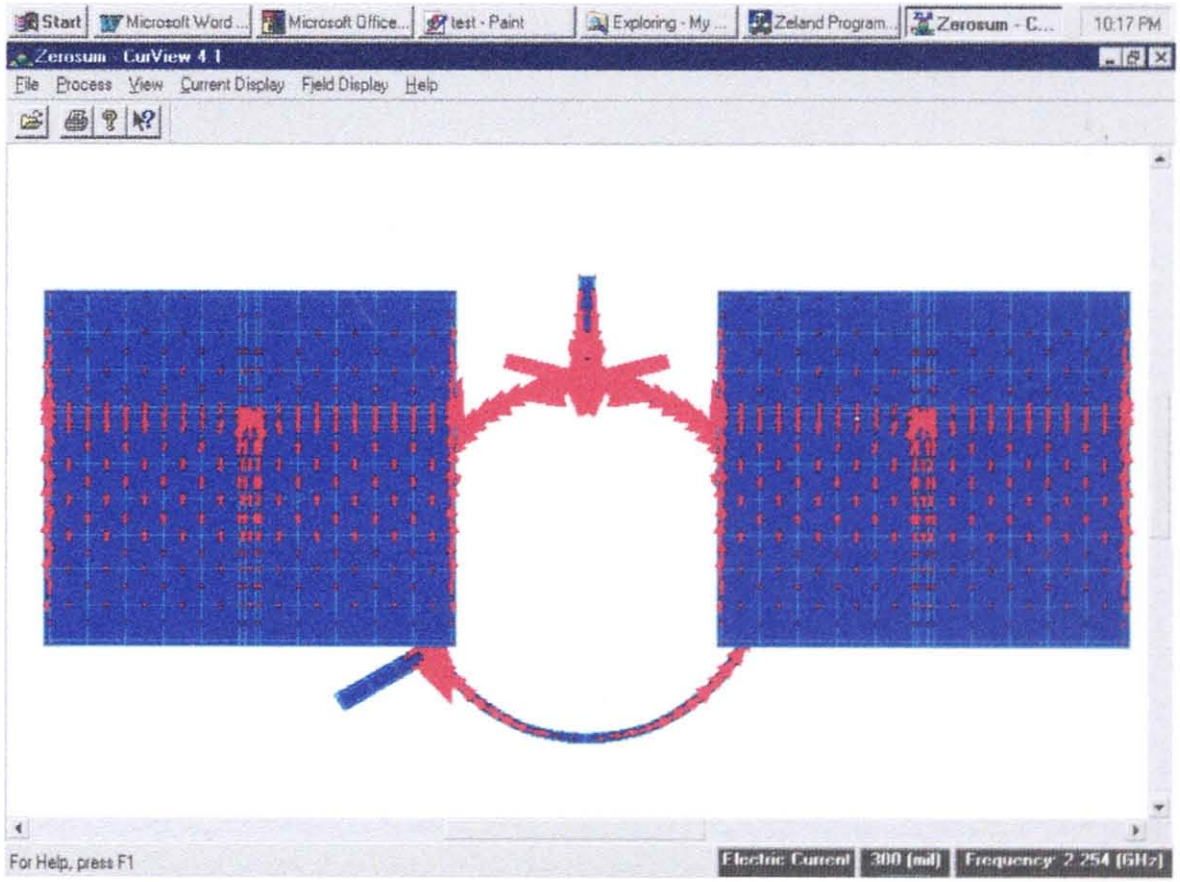

Figure 5.11 Current vector distribution of a zero-sum antenna excited at Σ- ports

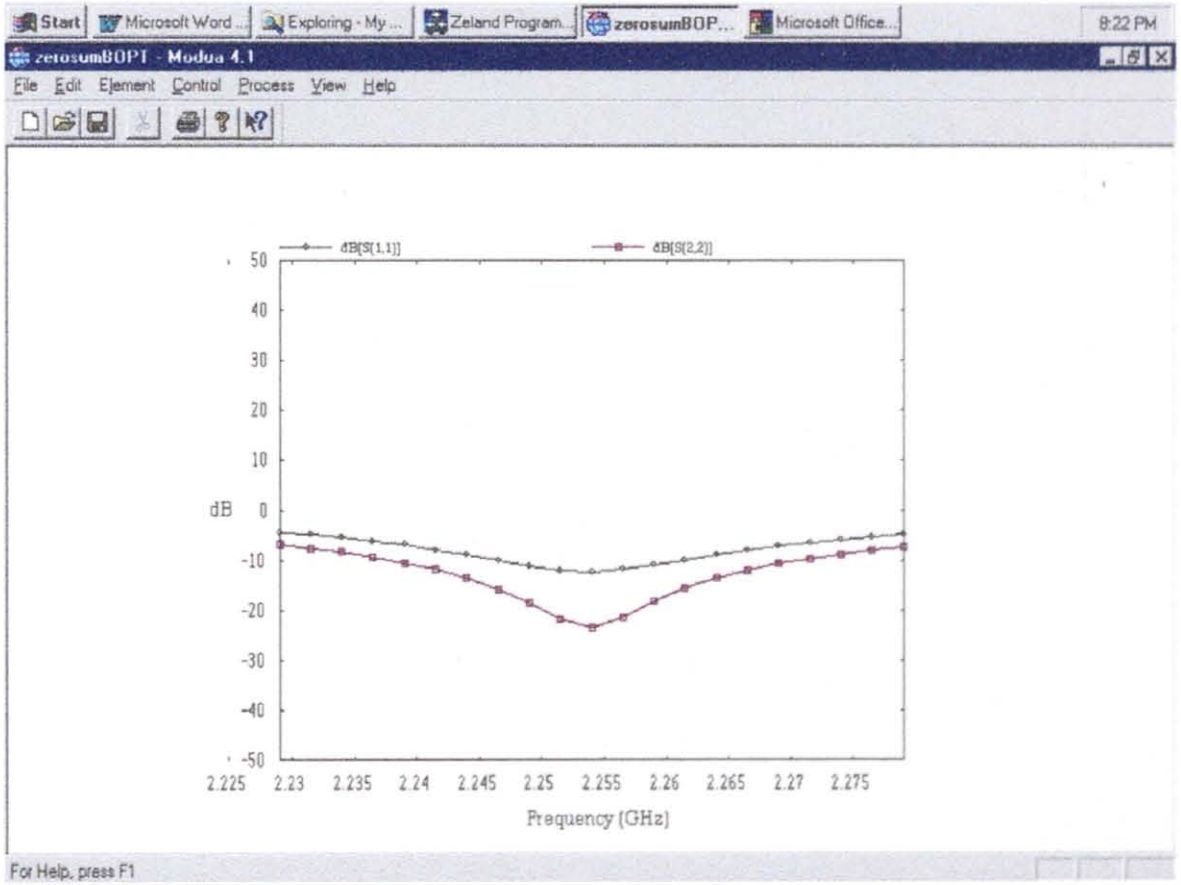

Figure 5.12 Simulated results of a return loss at port 1 (Σ-) and port 2 (Δ-) for the zero-sum antenna

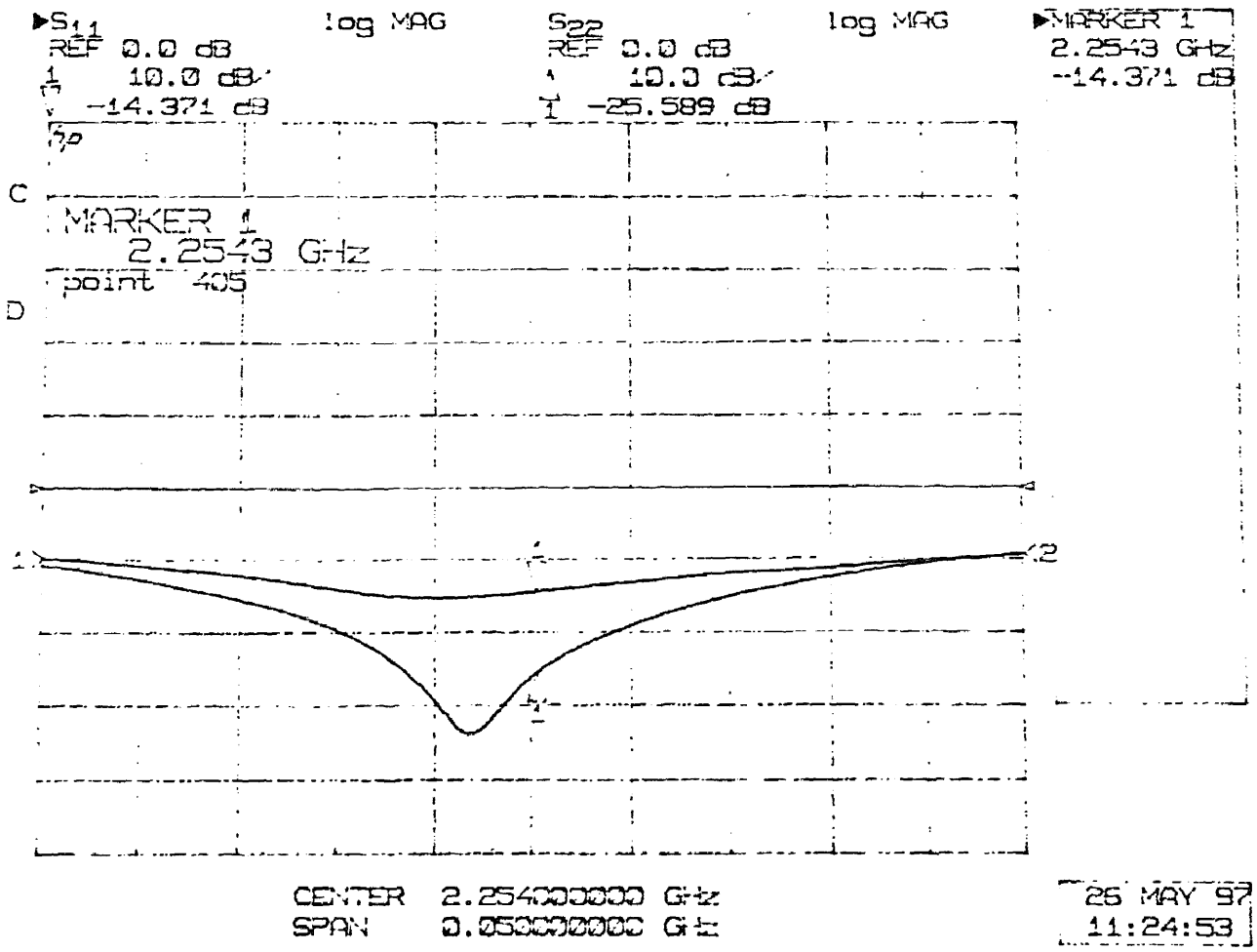

Figure 5.13 Experimental results of a return loss at a Σ - and a Δ - ports of the zero-sum antenna

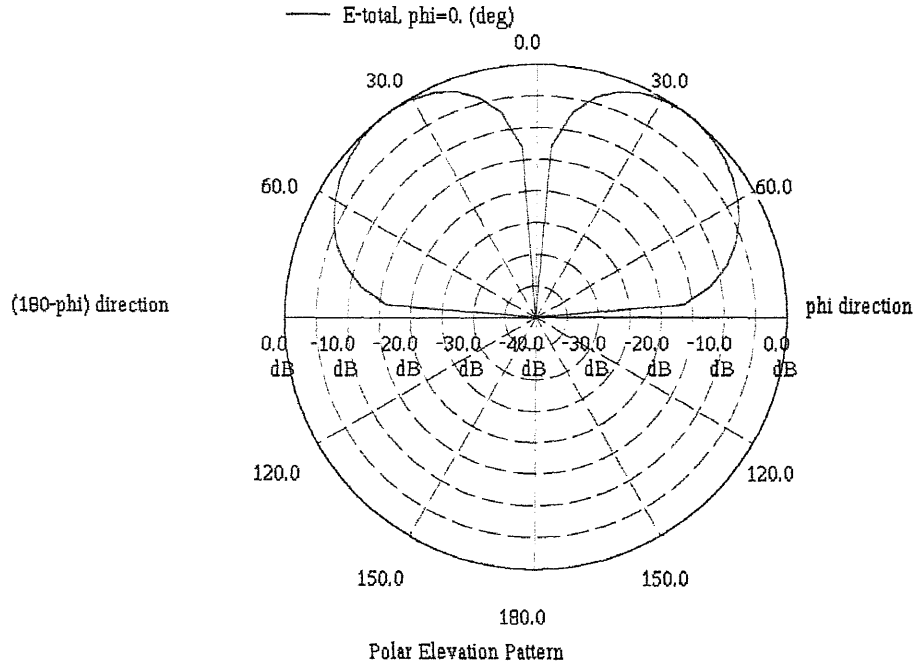

Figure 5.14 Simulated difference pattern of zero-sum antenna

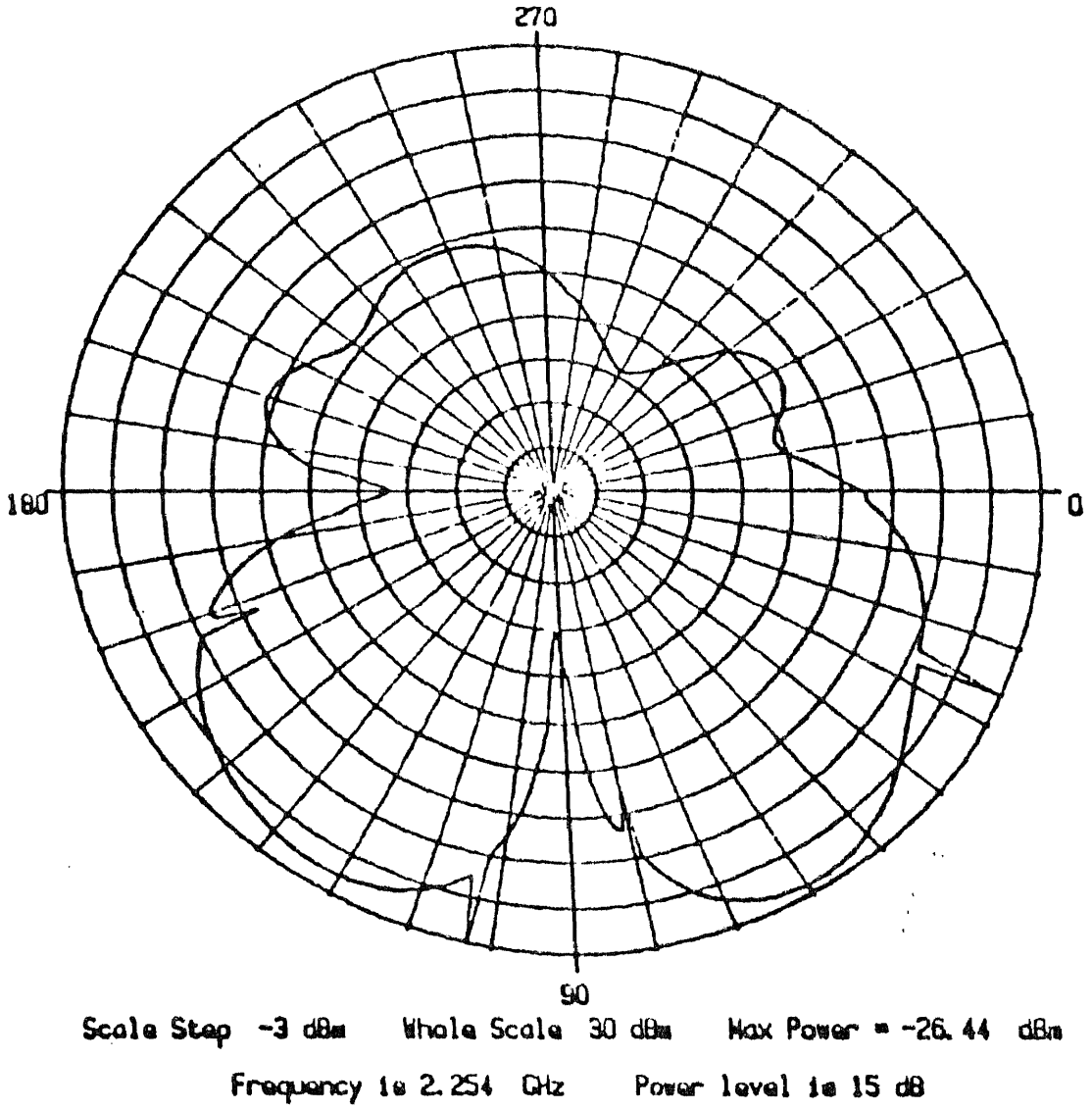

Figure 5.15 Experimental difference pattern of zero-sum antenna at f = 2.254 GHz

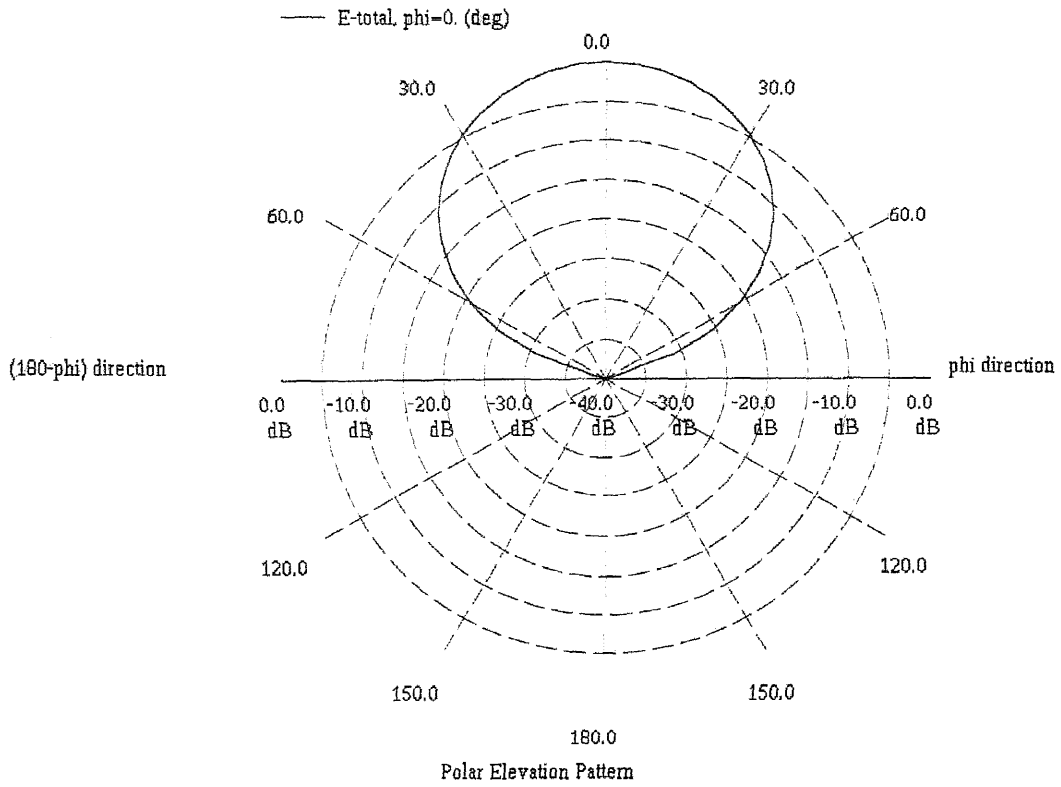

Figure 5.16 Simulated sum pattern of zero-sum antenna

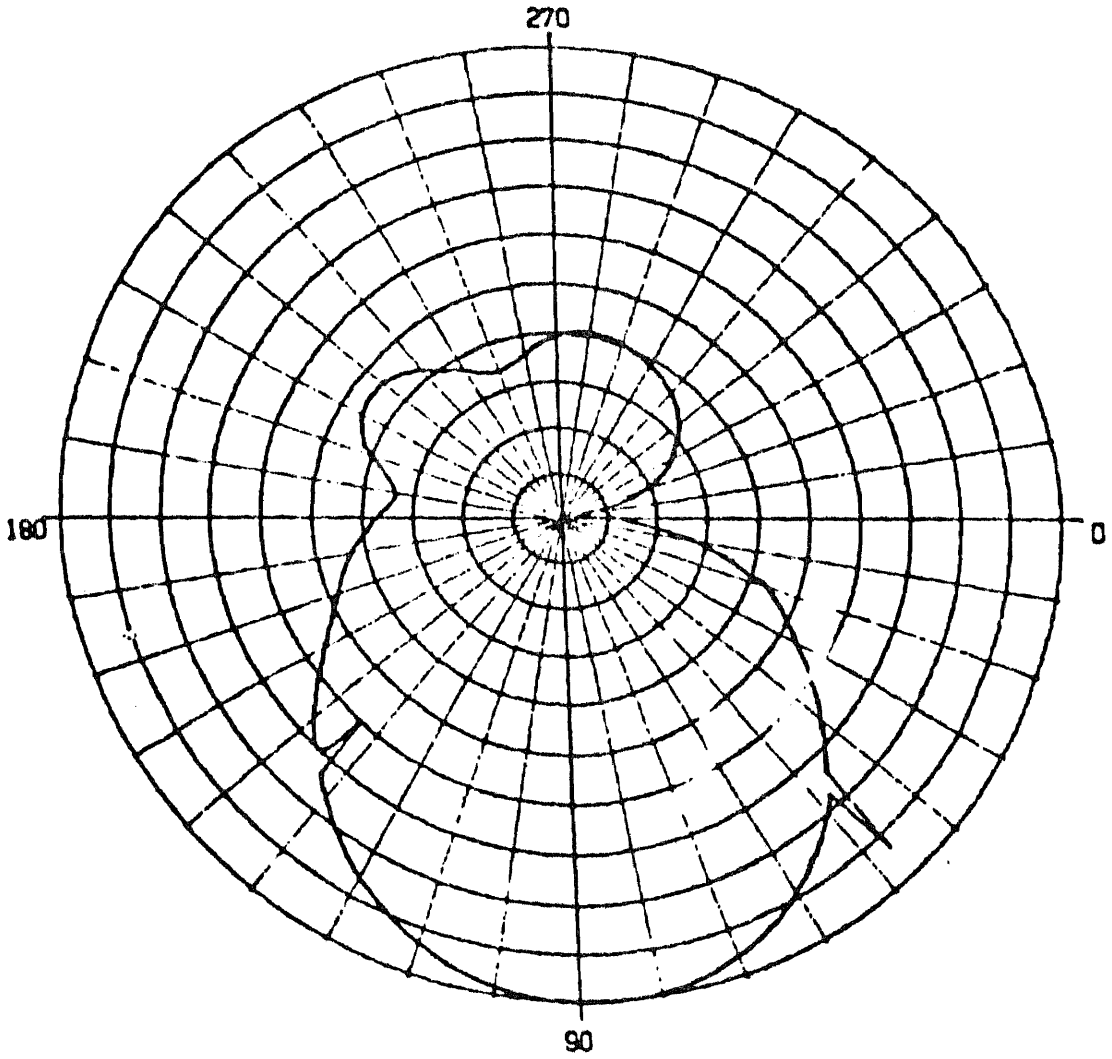

Figure 5.17 Experimental sum pattern of zero-sum antenna at f = 2.254 GHz

CHAPTER 6

CONCLUSIONS

A zero-sum antenna has been implemented as a combination of two element microstrip path antenna array and a hybrid (rat-race) ring coupler. Numerical optimization of feed location and patch size using IE3D electromagnetic simulation has been carried out for f = 2.254 GHz. Simulated results for a hybrid ring coupler demonstrated that sum and difference operations can be achieved with - 0.5 and - 40 dB levels, respectively, A zero-sum antenna simulation predicted that 40 dB difference is ideally possible between the sum and difference patterns in the forward direction. Experimental verification of the zero-sum antenna using MC5 material (ε_r=3.26 and h=60 mils) have shown that comparable performance can be achieved. The measured results for the sum and difference operation of a coupler were of the order of -2.5 and -2.2 dB whereas the difference between the main lobe and a null was of the order of -20 dB.

Further extension of this work could involve the study of the effects due to covering the zero-sum antenna by a radom. Another interesting application currently under investigation is the addition of the phase shifter into the zero-sum antenna to achieve beam scanning and direction finding for wireless indoor communication.

APPENDIX A

MC5 SPECIFICATION

GIL
Copper Clad Laminates

Glasteel Industrial Laminates
A Division of The Alpha Corporation
ISO 9002 Certified

MC5 High Frequency Laminate

Typical Properties of MC5

Description

Glasteel's new MC-5 copper clad laminate has been specifically designed for the high frequency circuit board market. MC-5 combines a high technology polyester resin with a state of the art continuous lamination process to produce a laminate with low and stable Dielectric constant (Dk) and Dissipation factor(Df). The Dk and Df remain stable over a broad temperature and humidity range when tested to 15 GHz.

Features and Benefits

- Dk and Df stable between -55 C & 125 C
- Dk and Df stable in dry and humid environments
- Fabrication in conventional PWB shops
- Standard FR4 drilling / cutting feeds and speeds
- No special through hole treatments
- Excellent mechanical properties
- Conventional glass construction
- Half ounce copper available
- No special storage requirements
- Standard assembly techniques
- UL 94 V-0 flammability rating
- Oxygen Index 49%
- Absolutely the best cost performance available

Electrical Properties

	Frequency	@ -55 C	@ 20 C	@ 125 C
Dielectric Constant	1 to 15 GHz	3.26 ± .05	3.26 ± .05	3.26 ± .05
Dissipation Factor [1] (See Graph on next page)	1 GHz	0.0012	0.0012	0.0012
	10 GHz	0.0015	0.0015	0.0015
	15 GHz	0.0022	0.0022	0.0022
Surface Resistivity	C/96/35/90		Megohm	4×10^4
Volume Resistivity	C/96/35/90		Megohm-cm	2×10^5
Moisture Insulation Resistance	40 cycles -2°C/90% RH to 65 C/95% RH		Megohm	7×10^4
Solvent Extract Conductivity	--		µp/cm	0.10

Physical Properties

Copper peel strength (1 oz copper)	Condition A	Lb/inch width	5.0
	After 20 sec @ 500 F	Lb/inch width	5.0
	@250 F	Lb/inch width	5.0
Flexural Strength, Length	Condition A	PSI	40,000
Flexural Strength, Cross	Condition A	PSI	38,000
Flexural Modulus, Length	Condition A	MPSI	2.1
Flexural Modulus, Cross	Condition A	MPSI	2.1
Moisture Absorption	D 24/23	%	0.17

Thermal Properties

Glass Transition Temperature	Condition A	°C	145
Thermal Stress	@ 500 F	seconds	60+
Z Axis Expansion RT - T_g	Condition A	ppm/°C	80
Z Axis Expansion T_g - 260 C	Condition A	ppm/°C	315
X/Y Axis Expansion	Condition A	ppm/°C	25 / 28
Thermal Conductivity	@ 70 C	W/m/K	0.228

Properties based on laminate with a nominal thickness of 0.030 inch (without copper)
[1] Data developed using microstrip technology

TSR-1346-H

178 Commerce Road • Collierville, Tennessee 38017 • 901 853 5070 • Fax 901-853-8884 • glam@o2net.com

APPENDIX B

DK AND DF VERSUS HUMIDITY

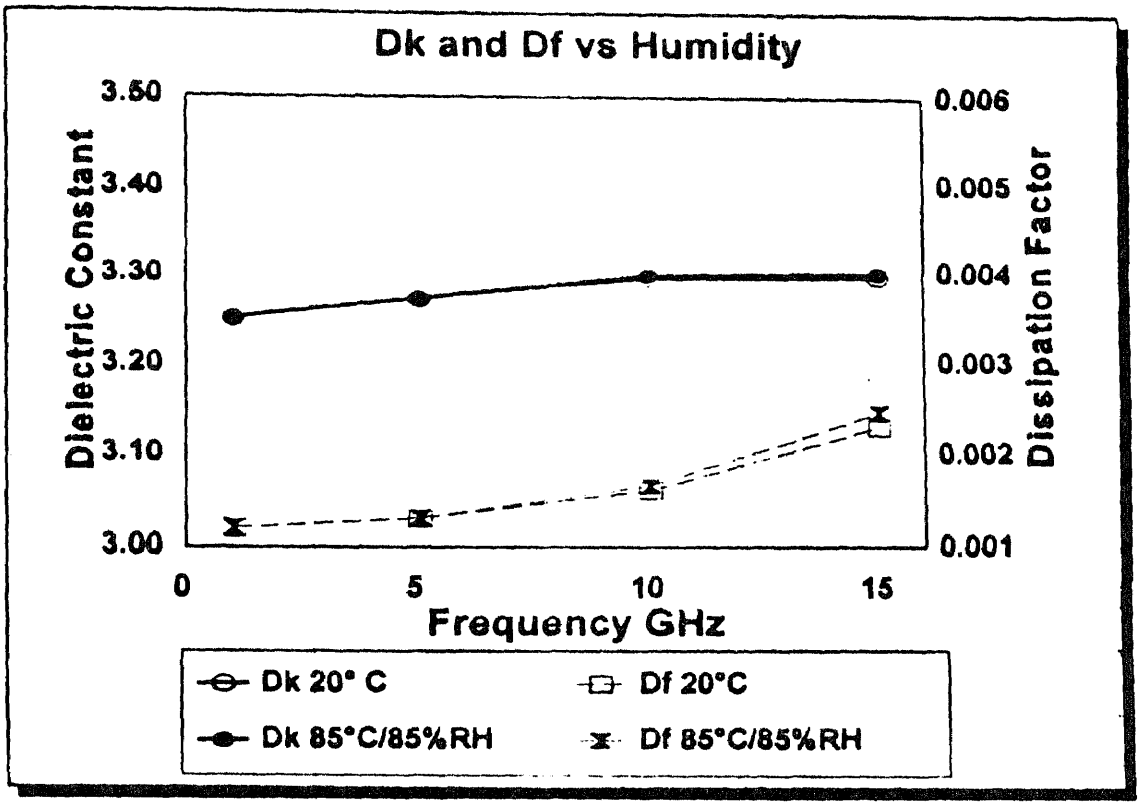

REFERENCES

[1] Matthaei, L. Young, and E.M.T. Jones., *Microwave filters, impedance-matching networks, and coupling structures*, Artch House, 1980.

[2] Warren L. Stutzman, and Gary A. Thiele, *Antenna Theory and Design*, John \Wiley &Sons, Inc., 1981, Chapter 3.

[3] *Mathematica version 2.2., The student book,* Addison Wesley Publishing Company, 1994.

[4] Samuel M. Sherman., *Monopulse Principles and Techniques*, Artech house 1984. Chapter 2.

[5] Allen Taflove, *Computational Electrodynamics*, The Finite-Difference Time-Domain Method., Chapter 3, Artech House, 1995.

[6] *IE3D User Manual, version 4.1* , Zeland Software Inc., 1997

[7] Christos Christopoulos., *The Transmission-Line Modeling Method TLM.*, The IEEE PRESS, 1995.

[8] Contantine A. Balanis., *Antenna Theory Analysis & Design*, John Wiley & Sons, Inc., 1997, Chapter 14.

[9] Bahl, I.J., and D.K. Triveli, A Designer's guide to microstrip line. Microwaves, May 1997.

[10] Cohn, S., "Characteristic impedance of the shielded-strip transmission line," IRE Trans. Microwave Theory and Techniques, Vol. MMT-2, No. 7, p.52, July 1954.

[11] E.O. Hammerstad, "Equation for Microstrip Circuit Design," Proc. Fifth European Microwave Conf., pp. 268-272, Sept. 1975.

[12] Derneryd, A., " A Theoretical Investigation of the Rectangular Microstrip Antenna Elements," IEEE Tran. On Antenna and Propagation, Vol. AP-26, pp 523-535, 1978.

[13] Lo, Y.T., D. Solomon and W.F. Richards, "Theory and experiment on Microstrip Antenna," IEEE AP-S Symposium (Japan), 1978, pp. 53-55.

[14] Pucel, Robert A., et al., Losses in microstrip. IEEE Trans. Microwave Theory and Techniques, Vol. MTT-16, No. 6, pp.342-350, June 1968.